APPENDIX B. DELFT3D FM MODEL CALIBRATION

This appendix provides details for the calibration efforts and results of the Delft3D Flexible Mesh model that was developed as part of the Coastal Systems Modeling Framework for the Partnership for Our Working Coast project. This appendix supports the Delft3D FM Model Calibration section of this report by providing additional maps and the timeseries, statistics, and tables that served as objective and quantitative measures for assessing model performance.

HYDRODYNAMICS

The hydrodynamics calibration is described separately for each parameter, i.e., water level, flow velocity, and waves, consistent with the model calibration steps.

Water Level

Calibration of water levels was performed primarily by adjusting the offshore water level boundary and changing the Delft3D FM wind drag coefficient. Model skill was assessed by comparing modeled versus measured water levels at open water and wetland gauges for quiescent conditions, cold fronts, and tropical cyclones. Additionally, observed and model predicted tidal amplitudes were compared.

Offshore boundary conditions

Adjustments were made to the offshore water level boundary condition based on NOAA's records of monthly averaged water level fluctuations at Grand Isle, related to dynamics in ocean temperatures, salinities, winds, atmospheric pressures, and oceanic currents (NOAA, n.d.). The average seasonal cycle of these fluctuations is displayed in Figure B-1. Figure B-2 shows the monthly deviation of recorded mean sea levels from the average seasonal cycle.

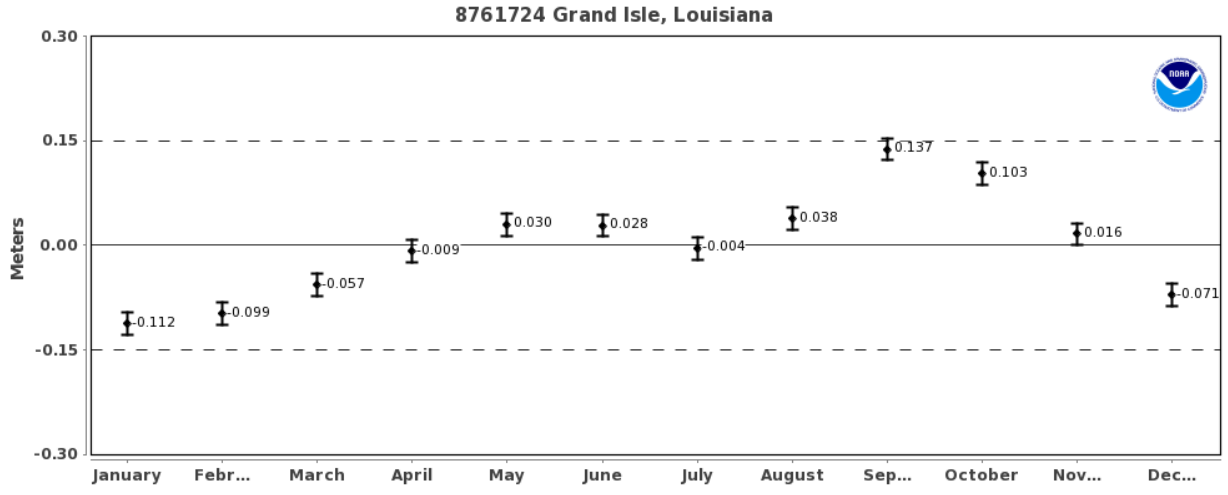

Figure B-1. Average seasonal cycle of mean sea levels at Grand Isle (NOAA, n.d.). Note the seasonal variation in mean sea level varies by ~0.25 m during the year.

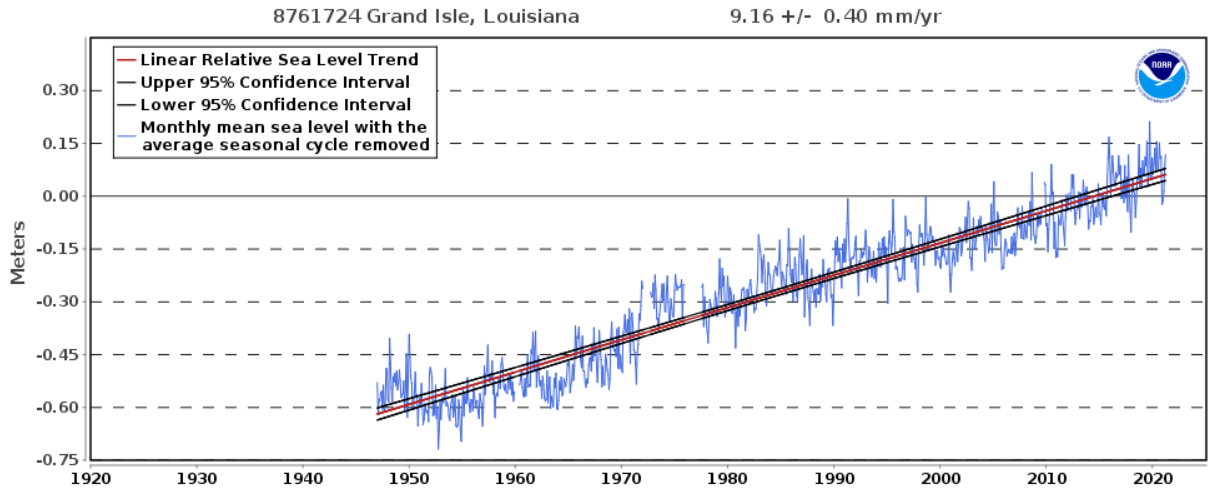

Figure B-2. Relative sea level trend at Grand Isle showing the monthly mean sea levels without the average seasonal cycle displayed in Figure B-1 (NOAA, n.d.).

Water Level Timeseries: Open Water Stations

This section compares modeled and measured water levels at open water gauges from USGS and NOAA located along Barataria Bay and Little Lake (Figure B-3). Timeseries comparisons are provided as daily averages during 2015, 2016, and 2019 (Figure B-4–Figure B-6), and as instantaneous timeseries for January 2015. Additionally, statistics are provided for instantaneous water levels during the entire year of 2019 (Figure B-7–Figure B-13).

The difference between the NOAA and USGS records at Barataria Pass at Grand Isle is caused by a discrepancy between vertical datum information provided by USGS and NOAA for their gauges at that location, which are located about 2 km apart. This discrepancy is suspected of causing the 20-30 cm water level difference that is found between the USGS and NOAA timeseries records at Grand Isle. Modeled water levels typically fall in between the records of both stations.

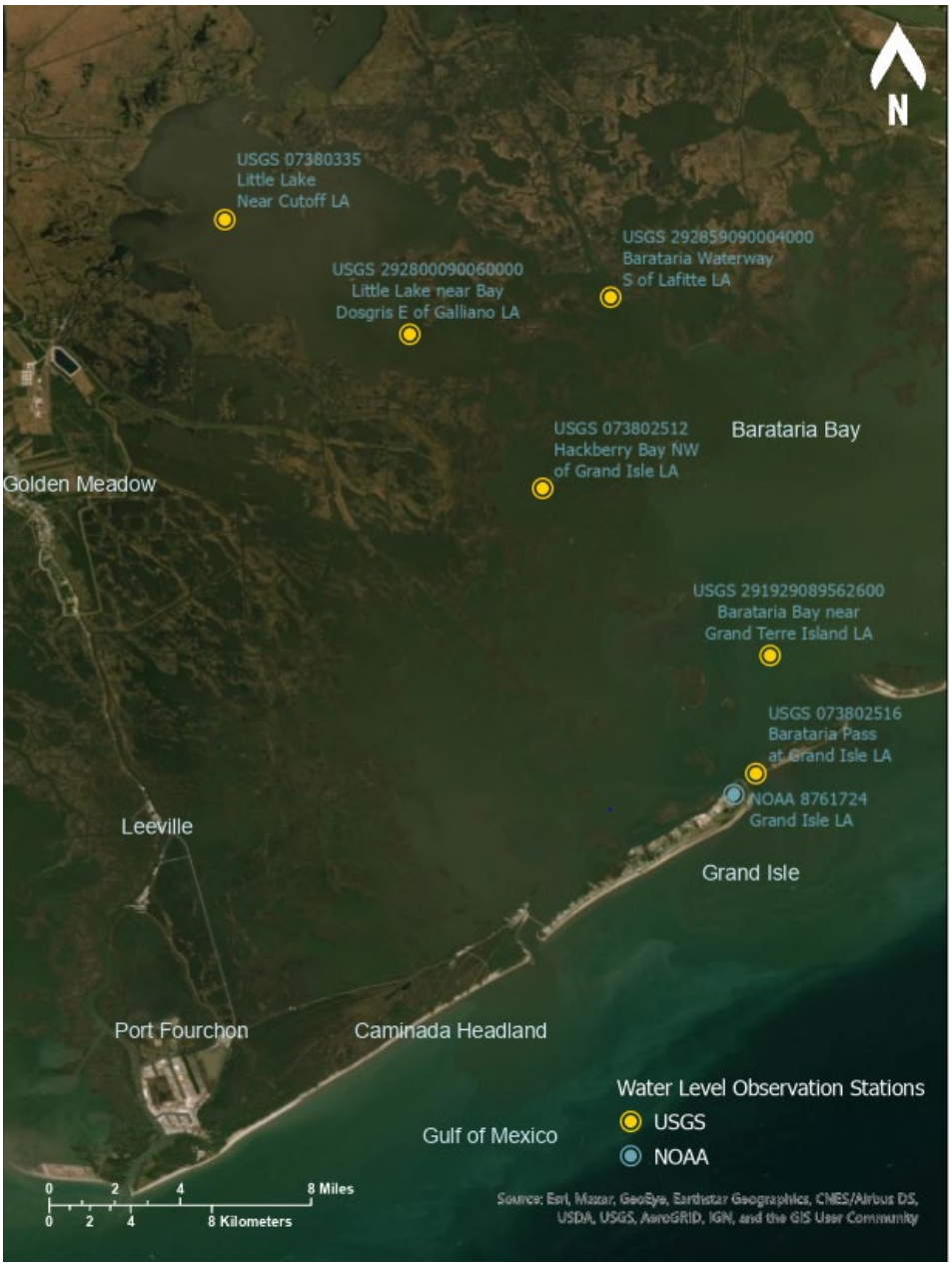

Figure B-3. Location of USGS and NOAA stations used in the model calibration of water level (Figure B-4 through Figure B-20)

Figure B-4. Daily average water levels at a transect through Barataria Basin for 2015. Model results are compared to USGS gage stations. The top left figure also shows the NOAA Grand Isle tide station in yellow.

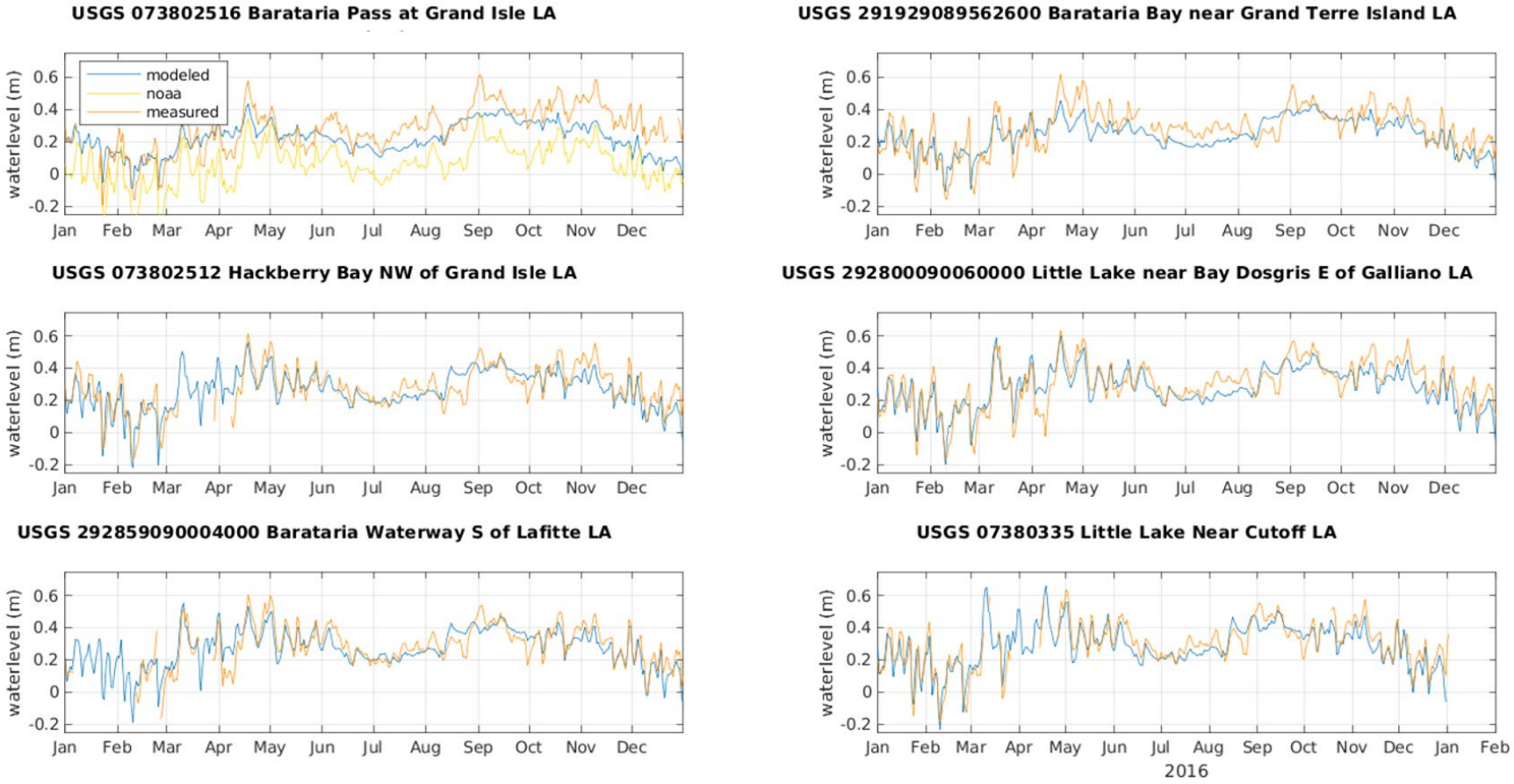

Figure B-5. Daily average water levels at a transect through Barataria Basin for 2016. Model results are compared to USGS gage stations. The top left figure also shows the NOAA Grand Isle tide station in yellow.

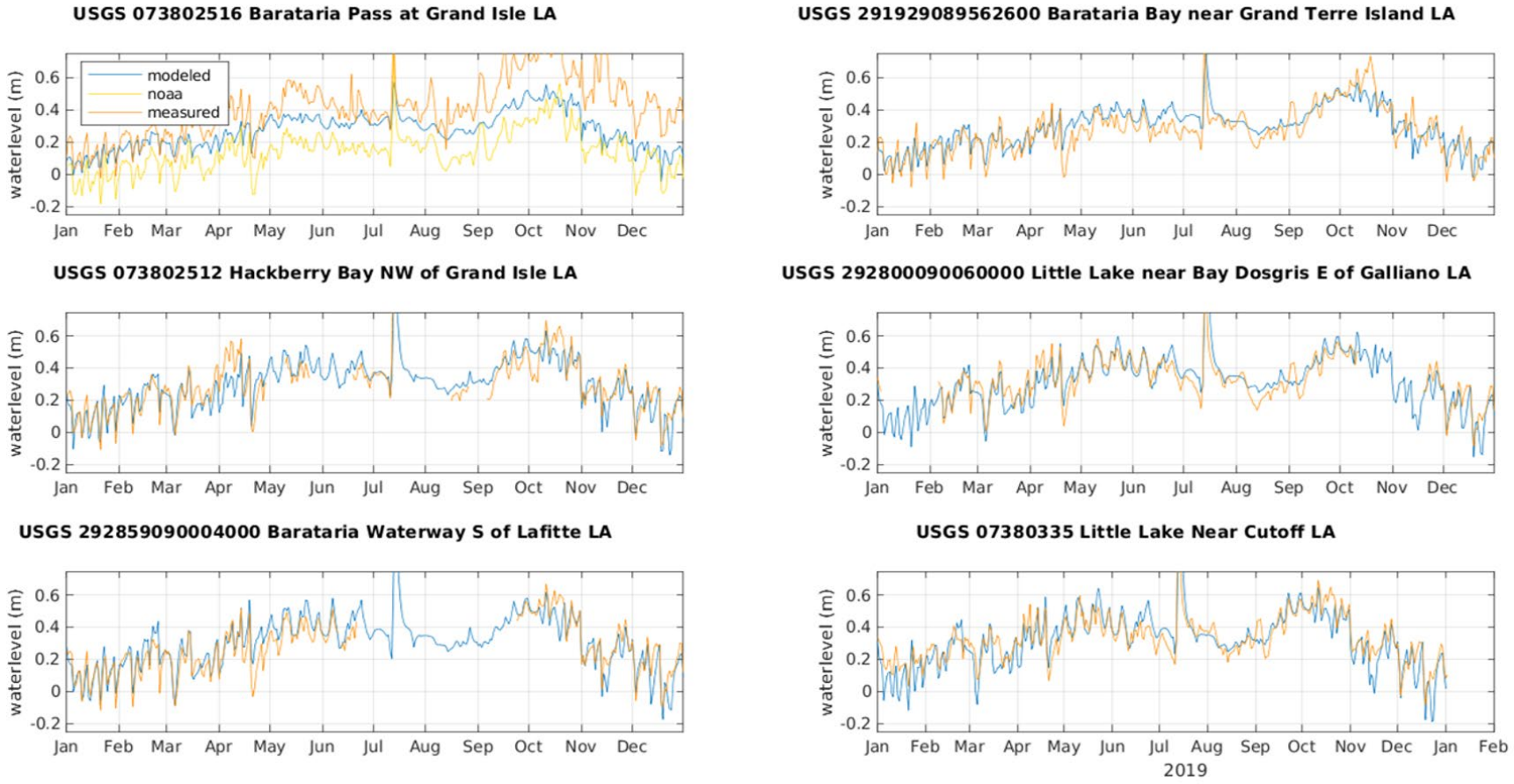

Figure B-6. Daily average water levels for a transect through Barataria Bay 2019. Model results are compared to USGS gage stations. The top left figure also shows the NOAA Grand Isle tide station in yellow.

Instantaneous timeseries

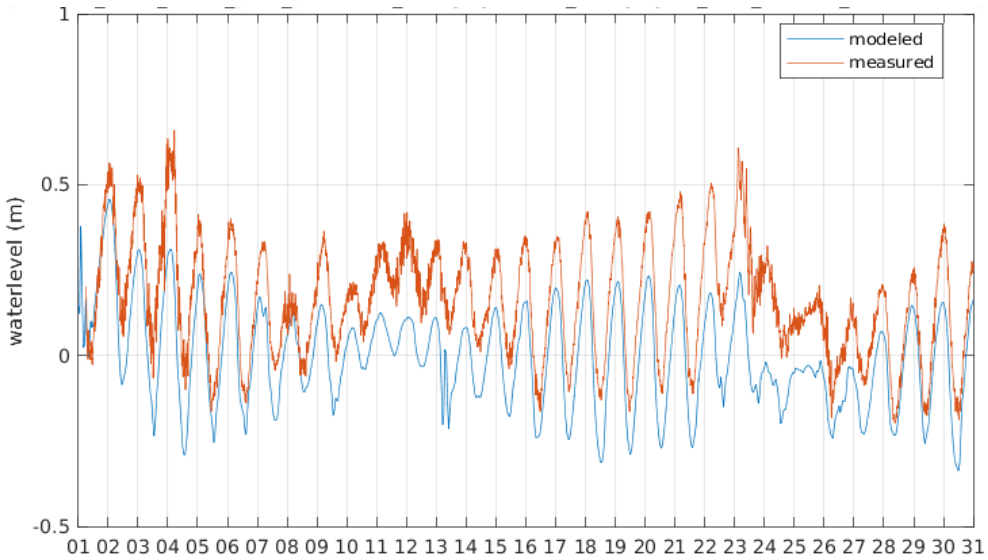

Figure B-7. Instantaneous water level comparison for January 2015 at USGS 073802516 Barataria Pass at Grand Isle

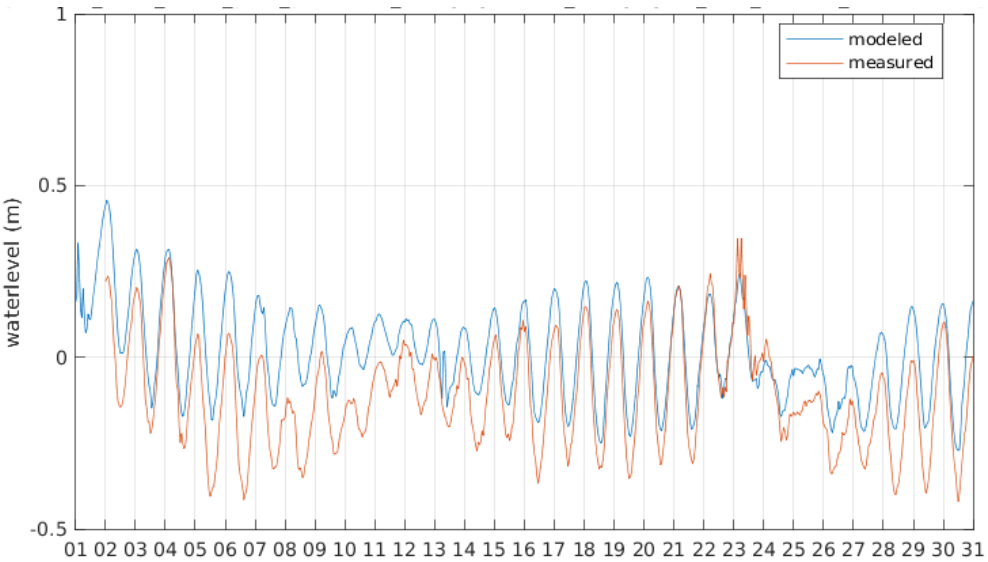

Figure B-8. Instantaneous water level comparison for January 2015 at NOAA Tide Gage 8761724 at Grand Isle

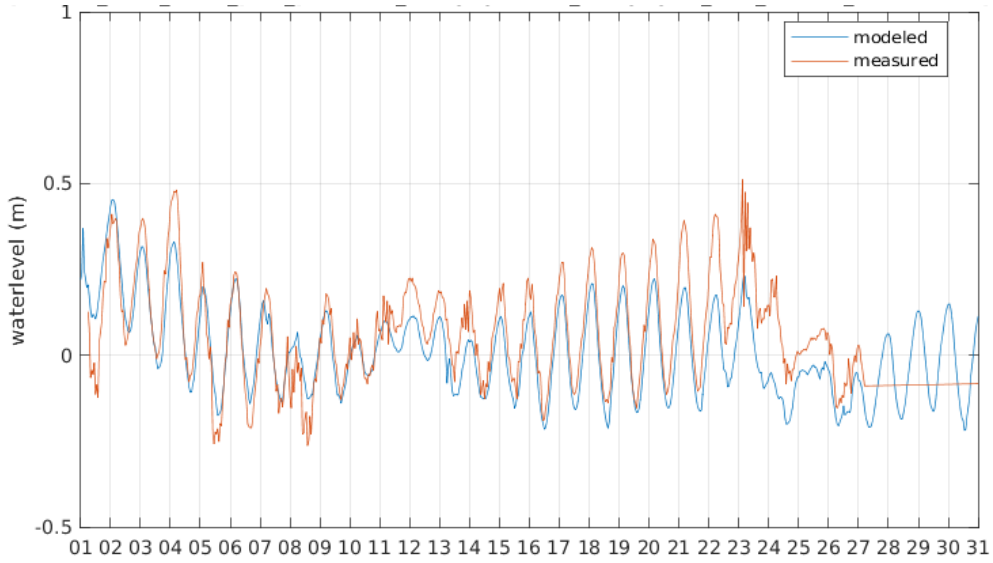

Figure B-9. Instantaneous water level comparison for January 2015 at USGS 291929089562600 Barataria Bay near Grand Terre Island

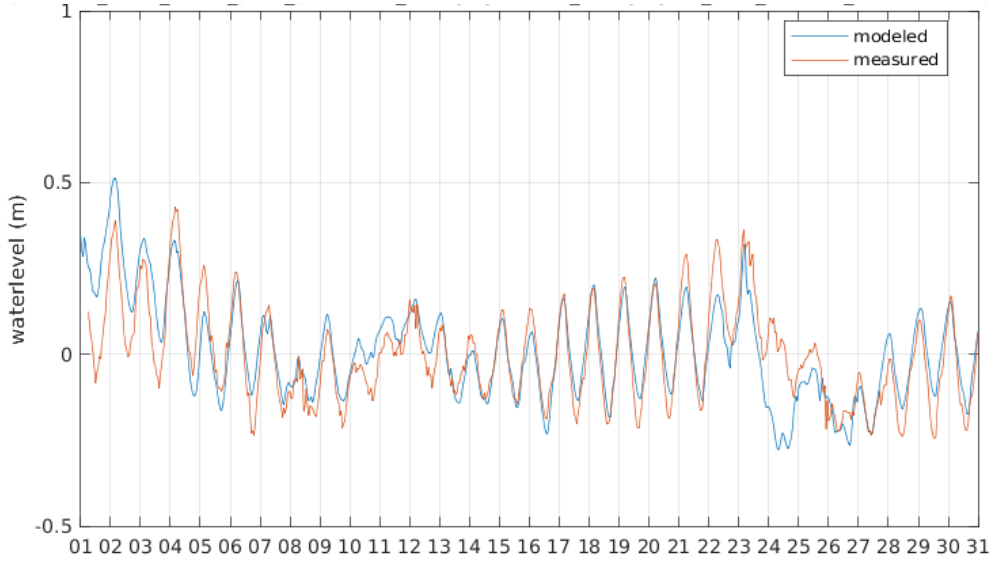

Figure B-10. Instantaneous water level comparison for January 2015 at USGS 073802512 Hackberry Bay NW of Grand Isle

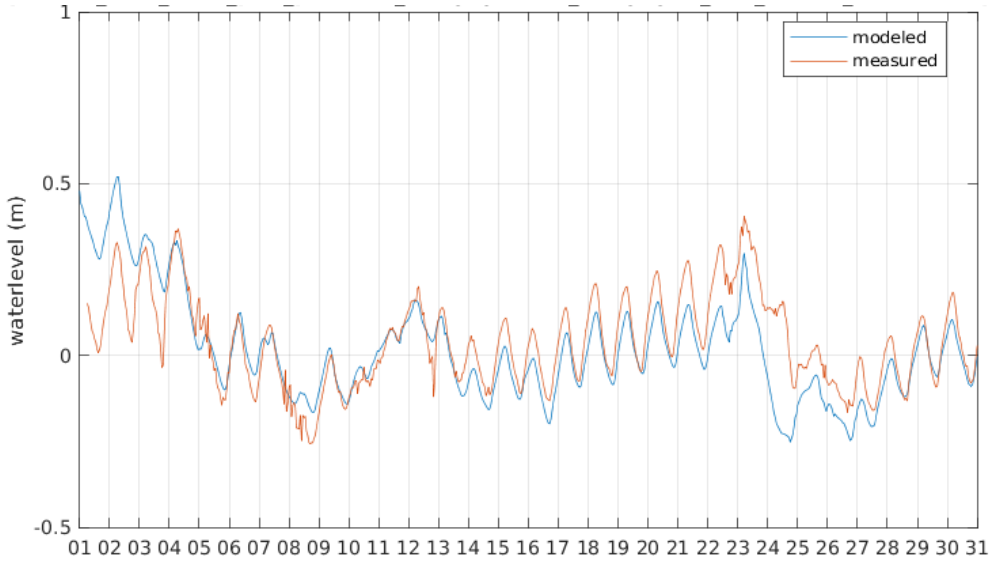

Figure B-11. Instantaneous water level comparison for January 2015 at USGS 07380335 Little Lake Near Cutoff

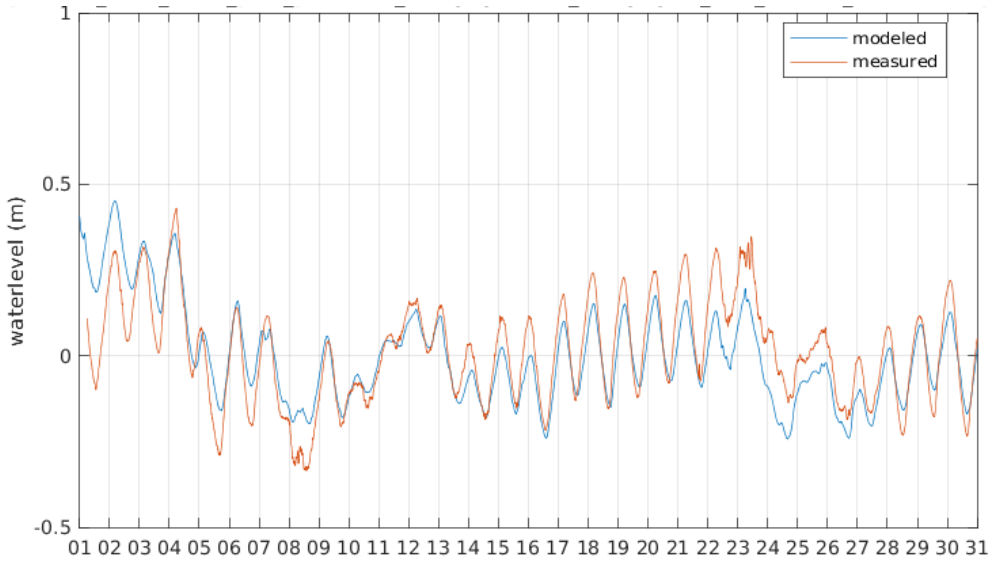

Figure B-12. Instantaneous water level comparison for January 2015 at USGS 292859090004000 Barataria Waterway S of Lafitte

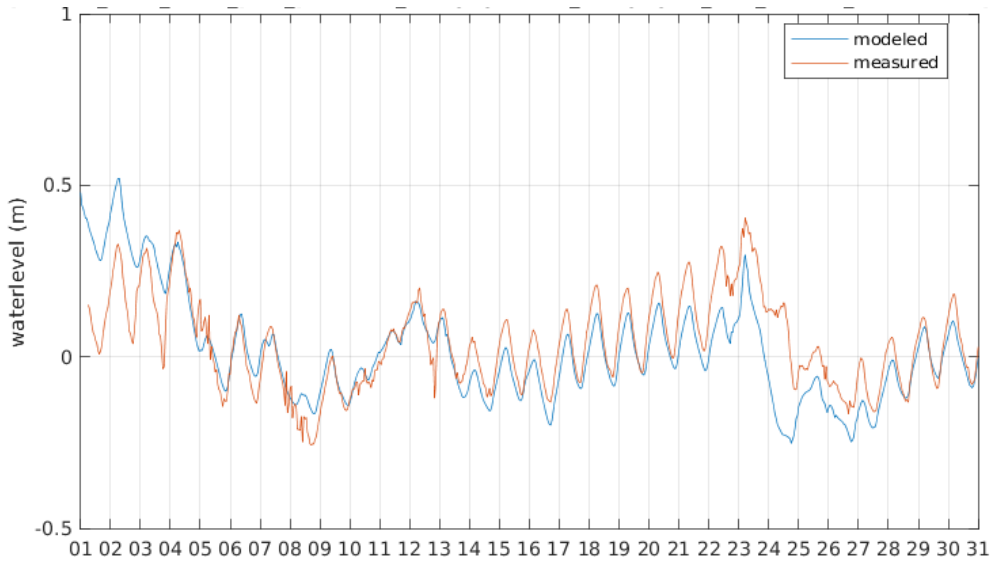

Figure B-13. Instantaneous water level comparison for January 2015 at USGS 07380335 Little Lake Near Cutoff

Water Level Statistics

Model skill was assessed quantitatively with several statistical measures calculated between modeled and observed data, i.e., the bias, root-mean-square error (RMSE), and the coefficient of determination (r^2), from which the correlation coefficient (r) can be determined. Figure B-14 through Figure B-20 show scatter plots of modeled and observed water levels, along with the statistical measures.

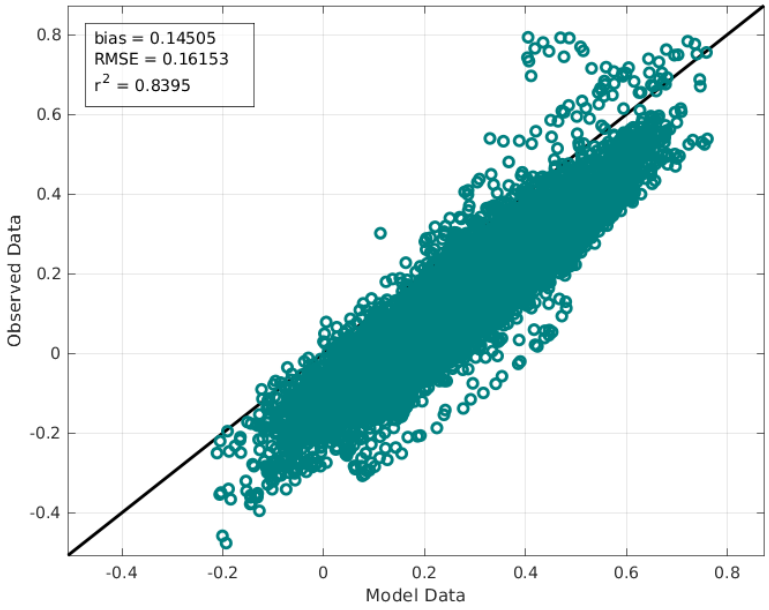

Figure B-14. Scatter plot between modeled and measured hourly water levels for 2019 at NOAA Tide Gage 8761724 at Grand Isle

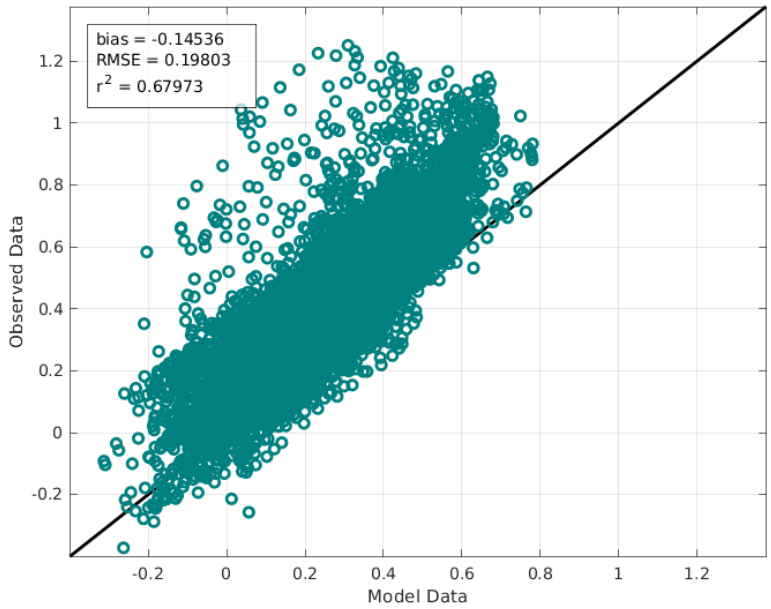

Figure B-15. Scatter plot between modeled and measured hourly water levels for 2019 at USGS 073802516 Barataria Pass at Grand Isle

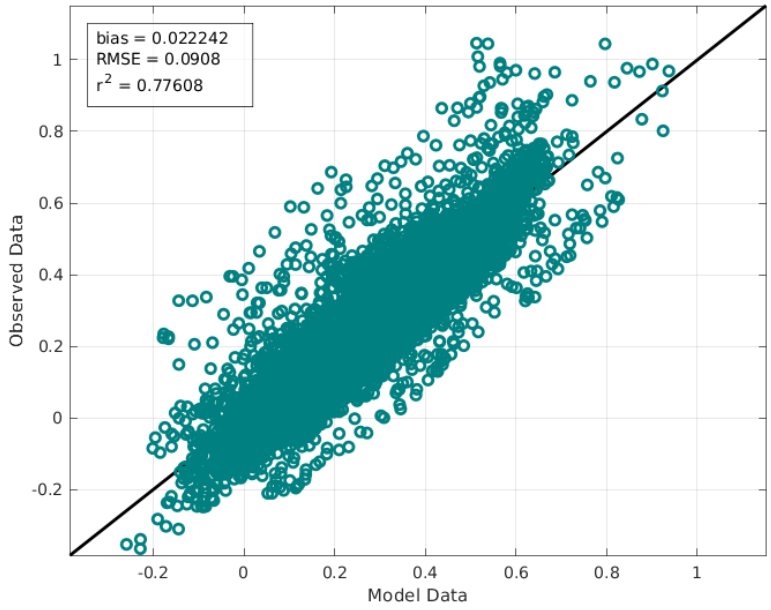

Figure B-16. Scatter plot between modeled and measured hourly water levels for 2019 at USGS 291929089562600 Barataria Bay near Grand Terre Island

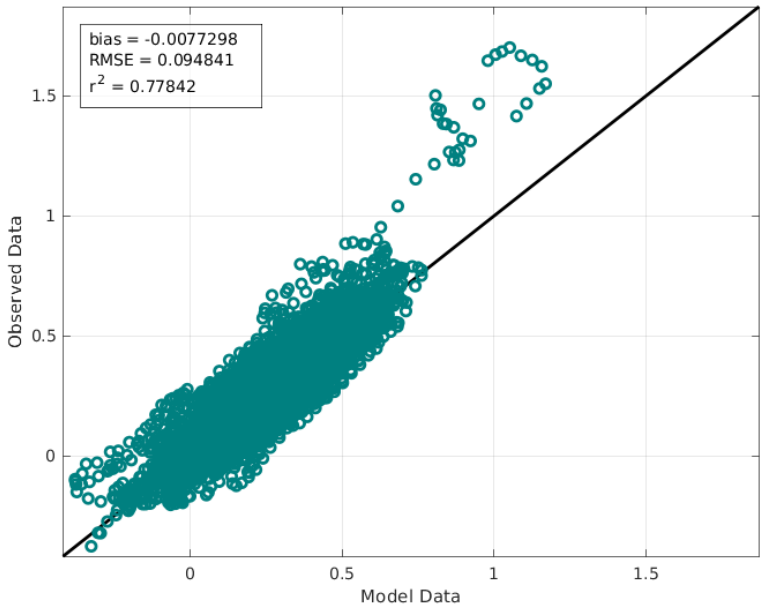

Figure B-17. Scatter plot between modeled and measured hourly water levels for 2019 at USGS 073802512 Hackberry Bay NW of Grand Isle

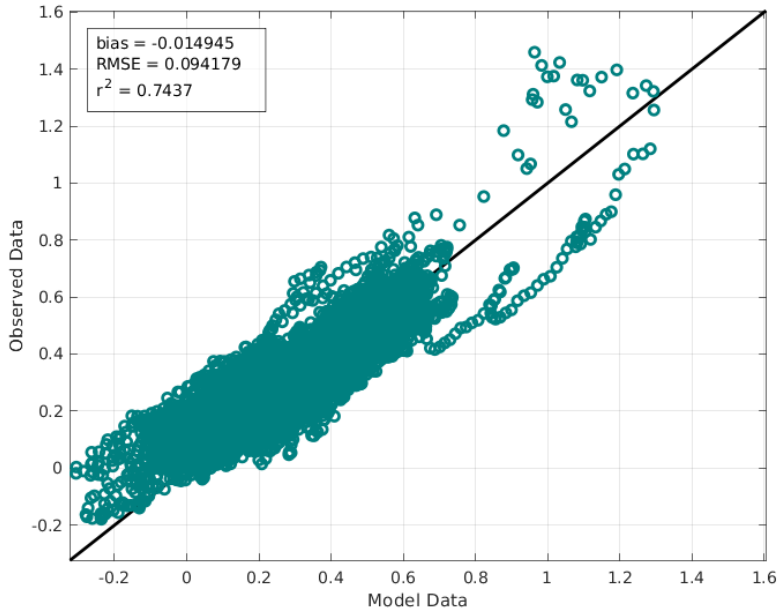

Figure B-18. Scatter plot between modeled and measured hourly water levels for 2019 at USGS 07380335 Little Lake Near Cutoff

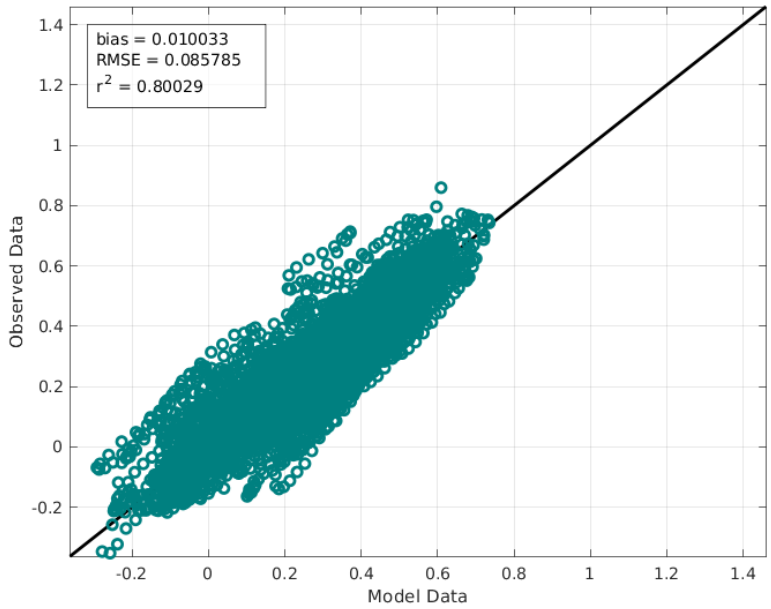

Figure B-19. Scatter plot between modeled and measured hourly water levels for 2019 at USGS 292859090004000 Barataria Waterway S of Lafitte

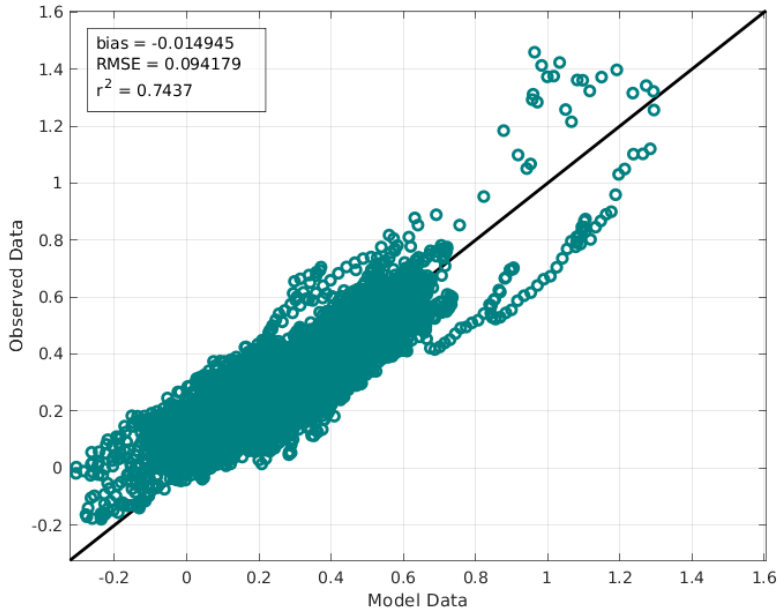

Figure B-20. Scatter plot between modeled and measured hourly water levels for 2019 at USGS 07380335 Little Lake Near Cutoff

Water Level Timeseries: Wetland Stations

This section compares modeled and measured water levels at wetland gauges located across the Barataria-Terrebonne Basin (Figure B-21), which are part of Louisiana's Coastwide Reference Monitoring System (CRMS)

Figure B-21. Location of CRMS stations for which timeseries figures are shown in Figure B-22 through Figure B-27.

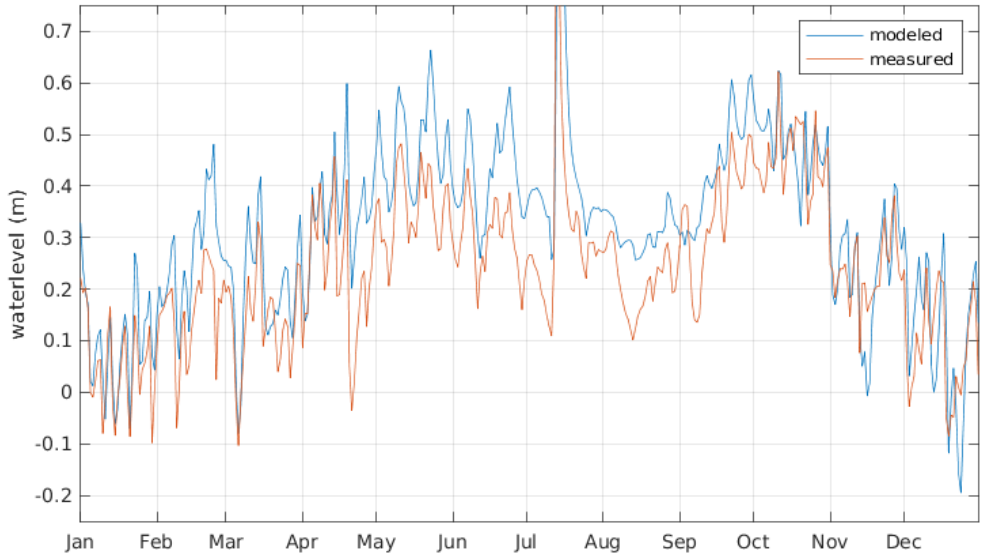

Figure B-22. Daily average water level comparison for 2019 for CRMS4218 located north of Little Lake, Barataria

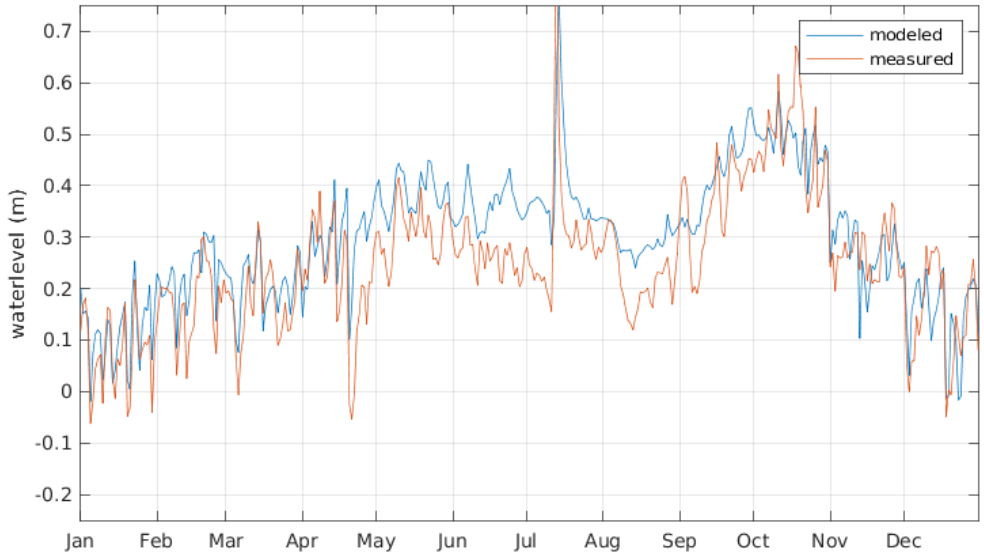

Figure B-23. Daily average water level comparison for 2019 for CRMS0178 located north of Grand Isle

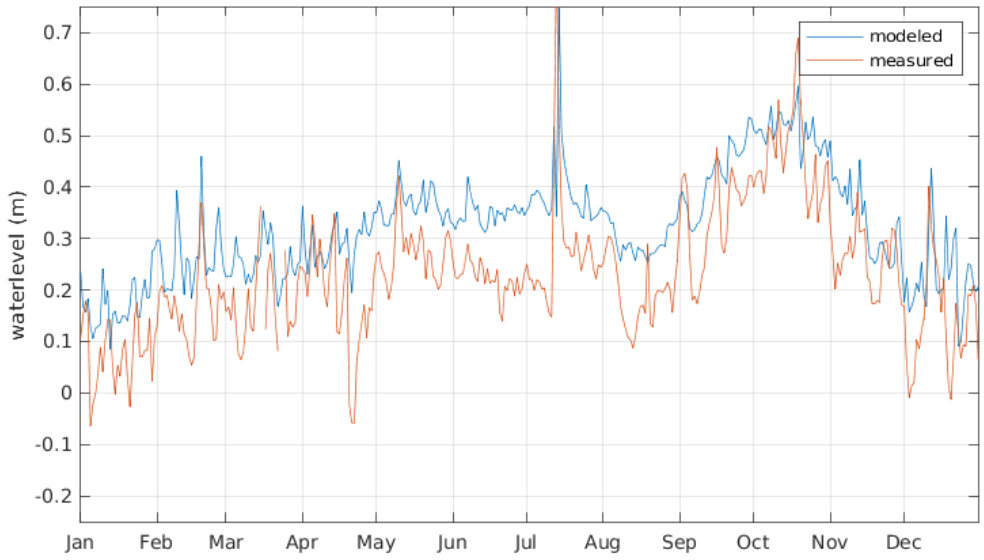

Figure B-24. Daily average water level comparison for 2019 for CRMS0164 located east of Hwy 1, near Port Fourchon

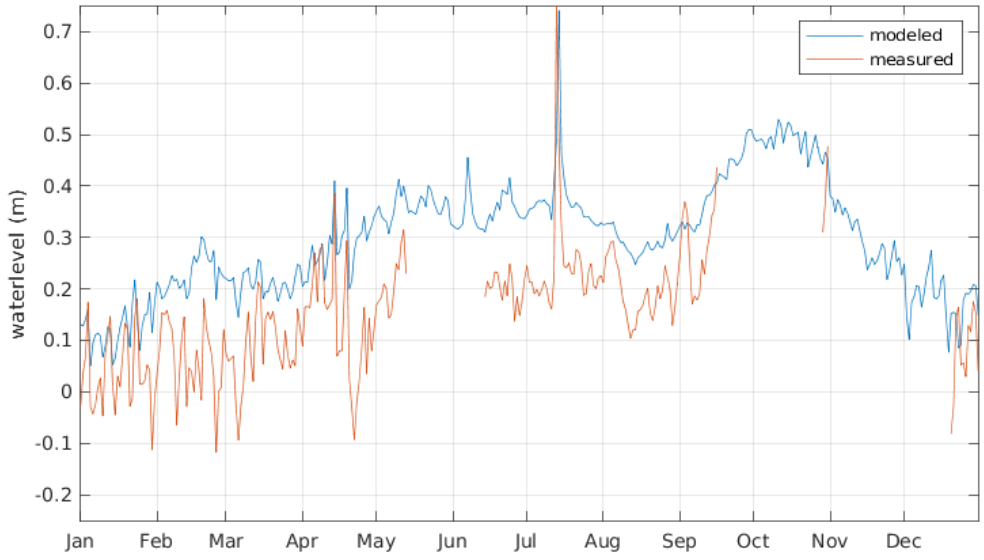

Figure B-25. Daily average water level comparison for 2019 for CRMS0292 located west of Bayou Lafourche, near Port Fourchon

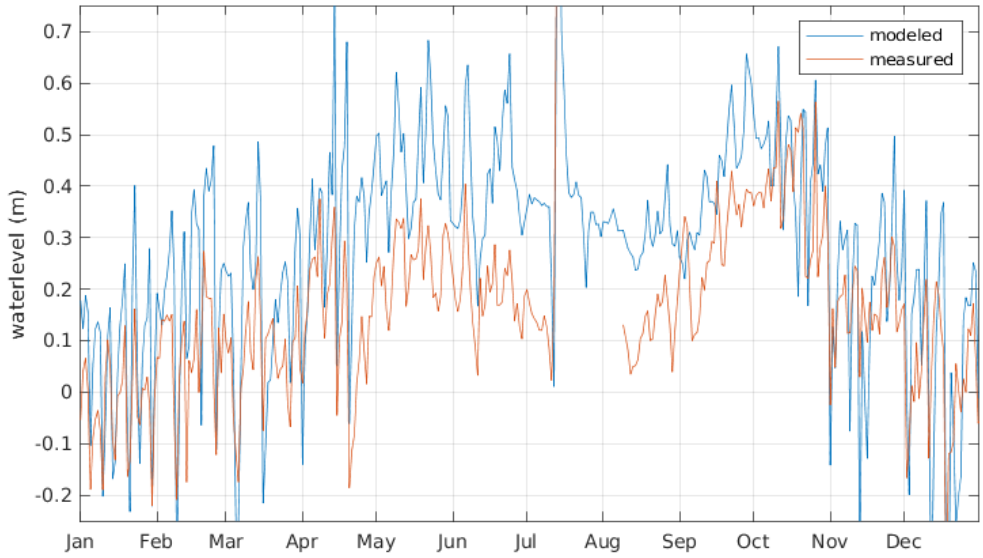

Figure B-26. Daily average water level comparison for 2019 for CRMS0341 located northwest of Terrebonne Bay

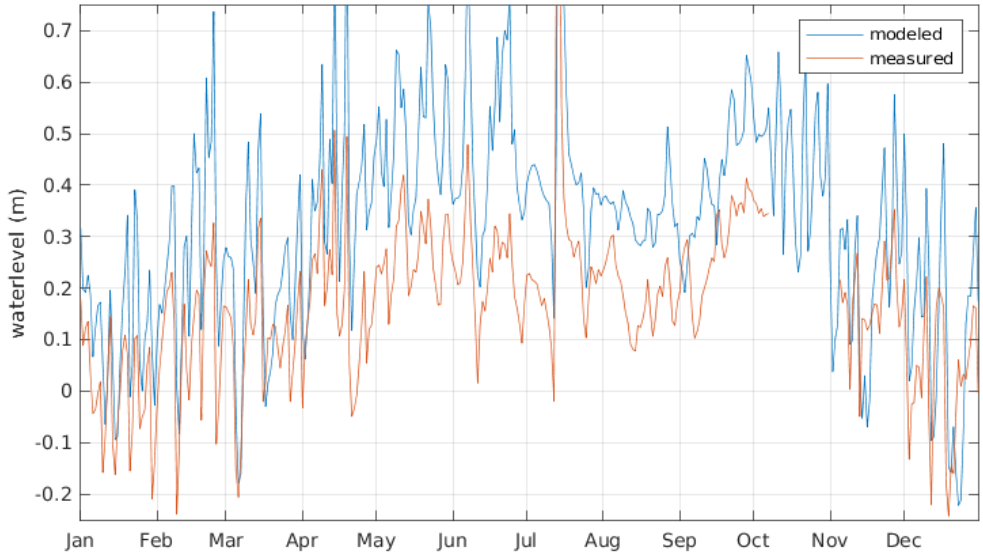

Figure B-27. Daily average water level comparison for 2019 for CRMS0386 located northwest of Golden Meadow

Water Level Timeseries: Tropical Cyclones

This section contains comparisons between modeled and measured water levels during tropical cyclones Katrina and Rita (Figure B-28 and Figure B-29) at the previously discussed open water gauges from USGS located along Barataria Bay and Little Lake (Figure B-3). Additionally, the comparisons include previous model results for the Advanced CIRCulation (ADCIRC) model (Cobell & Roberts, 2021).

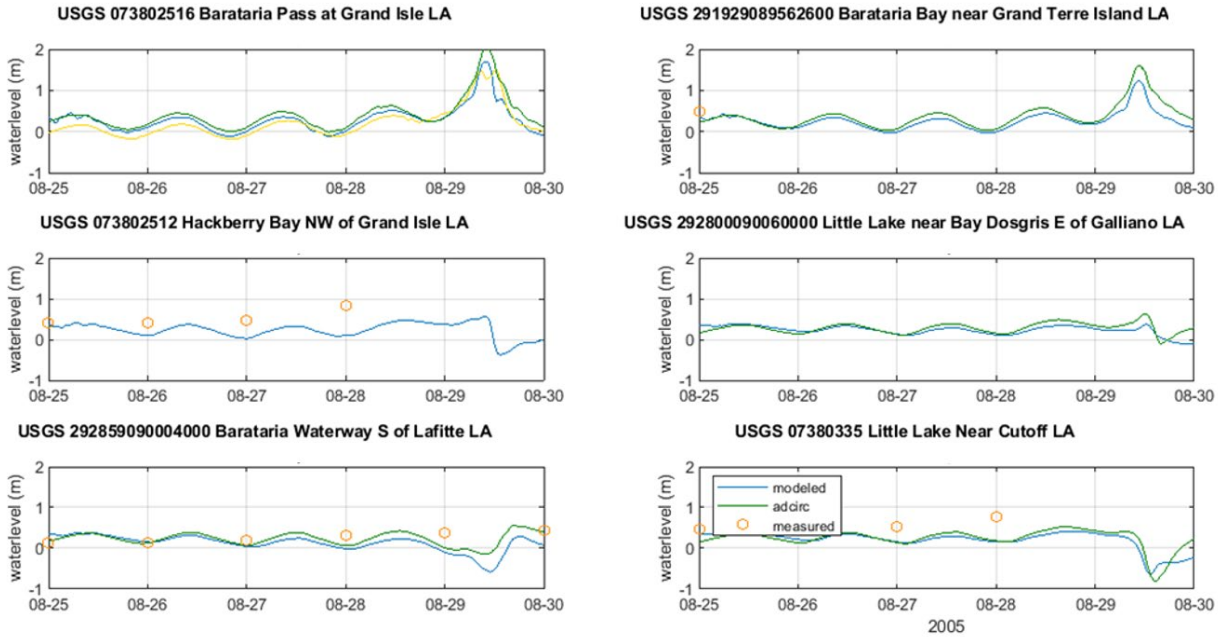

Figure B-28. Instantaneous water levels at the transect through Barataria Basin (locations indicated in Figure B-3) for Hurricane Katrina. Blue lines show results from the Delft3D FM model used in this study. Green lines show previous ADCIRC results from Cobell and Roberts (2021). The yellow line at the USGS Barataria Pass at Grand Isle represents measured hourly water levels at NOAA's station at Grand Isle. The orange circles indicate recorded daily maximum water levels, except for USGS Barataria Waterway S of Lafitte where these indicate daily mean water levels.

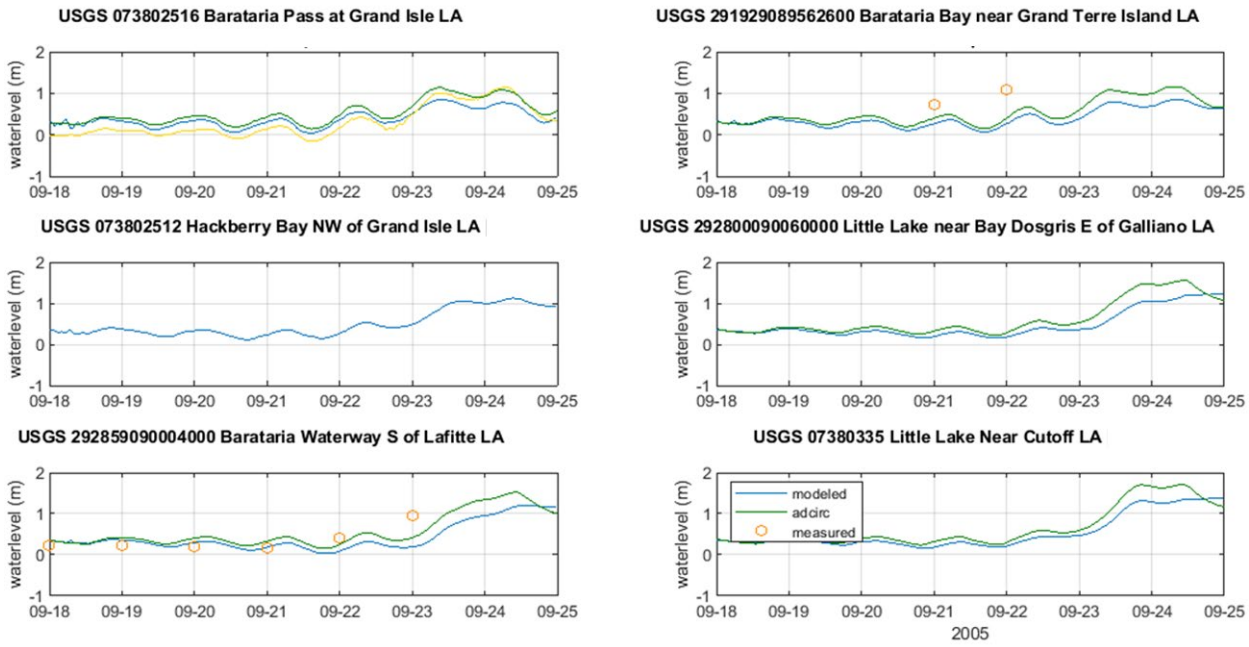

Figure B-29. Instantaneous water levels at the transect through Barataria Basin (locations indicated in Figure B-3) for Hurricane Rita. Blue lines show results from the Delft3D FM model used in this study. Green lines show previous ADCIRC results from Cobell and Roberts (2021). The yellow line at the USGS Barataria Pass at Grand Isle represents measured hourly water levels at NOAA's station at Grand Isle. The orange circles indicate recorded daily maximum water levels, except for USGS Barataria Waterway S of Lafitte where these indicate daily mean water levels.

Tidal Harmonics

A tidal harmonic analysis was performed on water levels modeled at NOAA stations (Figure B-30). Outcomes for all diurnal constituents, i.e., K1, O1, P1, Q1, were compared with decomposed harmonics derived for observations. Results are shown for the summation of the amplitudes of K1, O1, P1, Q1 in Figure B-31, which roughly equates to half of the maximum tidal range. The offset for Cocodrie is likely because the gauge is located at the edge of the model domain.

Figure B-30. Locations of NOAA stations for which a tidal harmonics analysis was performed

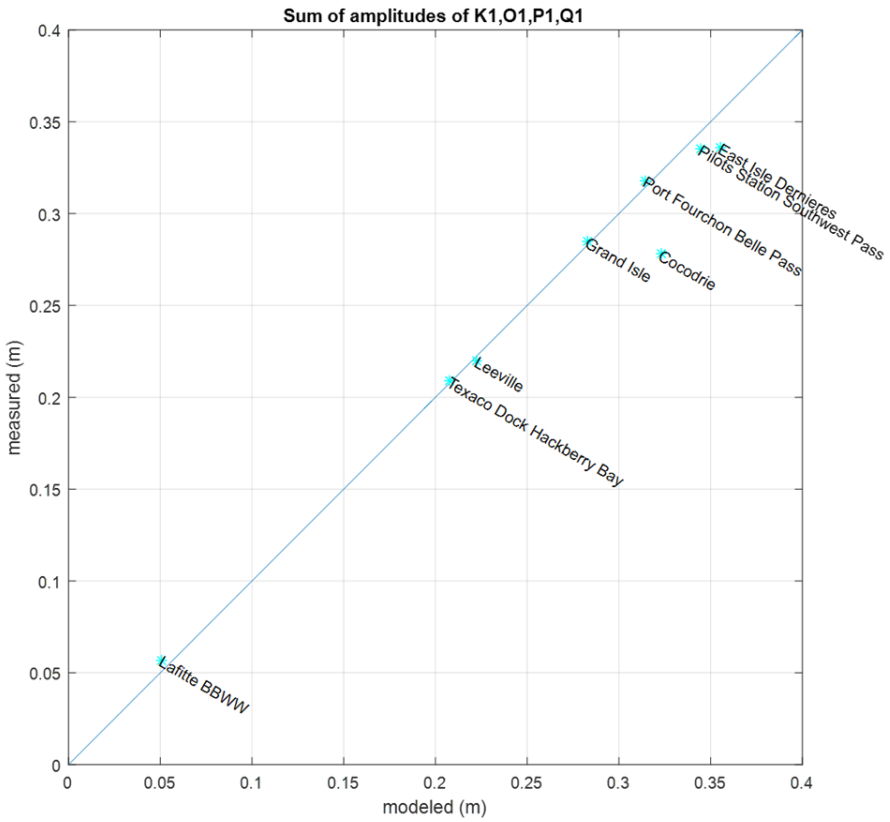

Figure B-31. Modeled vs. measured comparison of the summed tidal amplitudes K1, O1, P1, Q1 for stations indicated in Figure B-30. Tidal harmonic analysis was performed using T_TIDE (Pawlowicz et al., 2002).

Flow Velocity

Flow velocities in tidal inlets, channels, and bayous, were inspected to ensure they fell within typical ranges for the area of interest based on hydraulic stability curves for inlets (Figure B-32 and Figure B-33; Escoffier, 1940) and as reported in previous studies (Huang & Li, 2020).

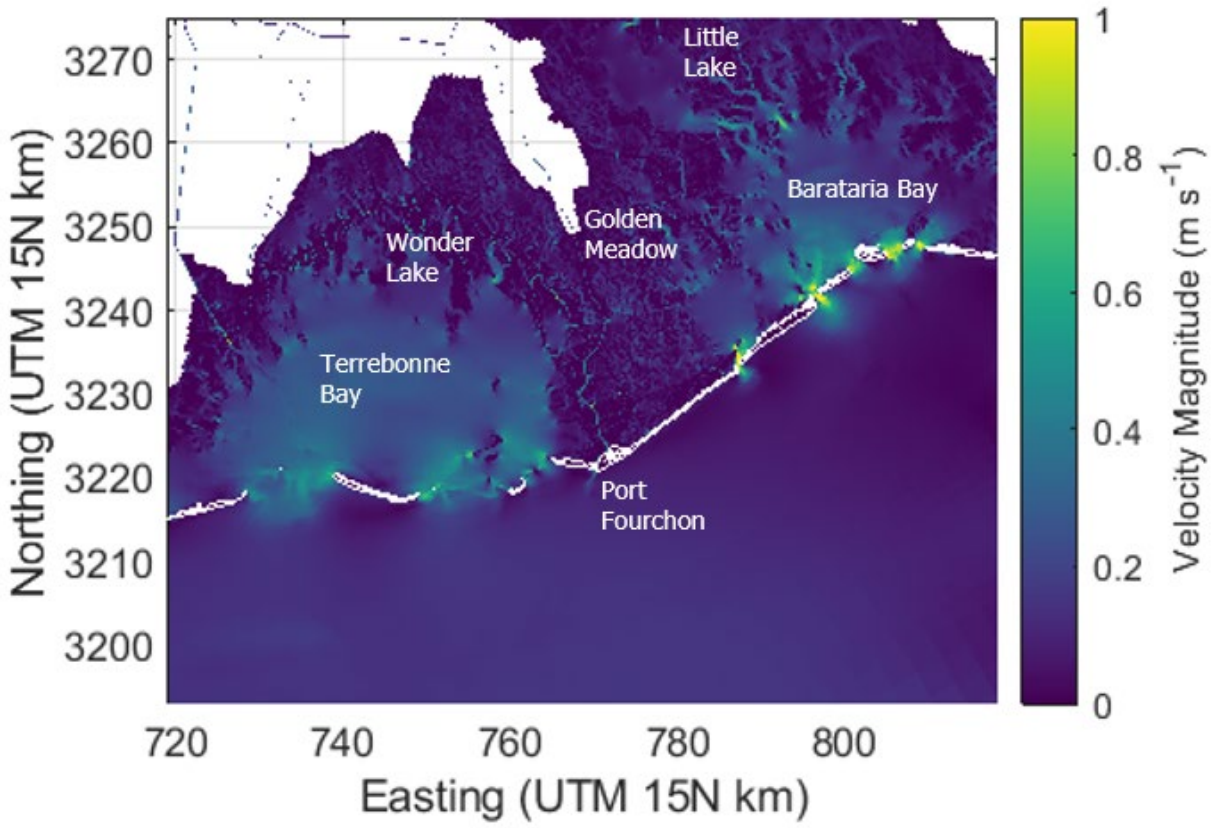

Figure B-32. Modeled flow velocities during a spring ebb tide at 12:00 PM on January 4th, 2015

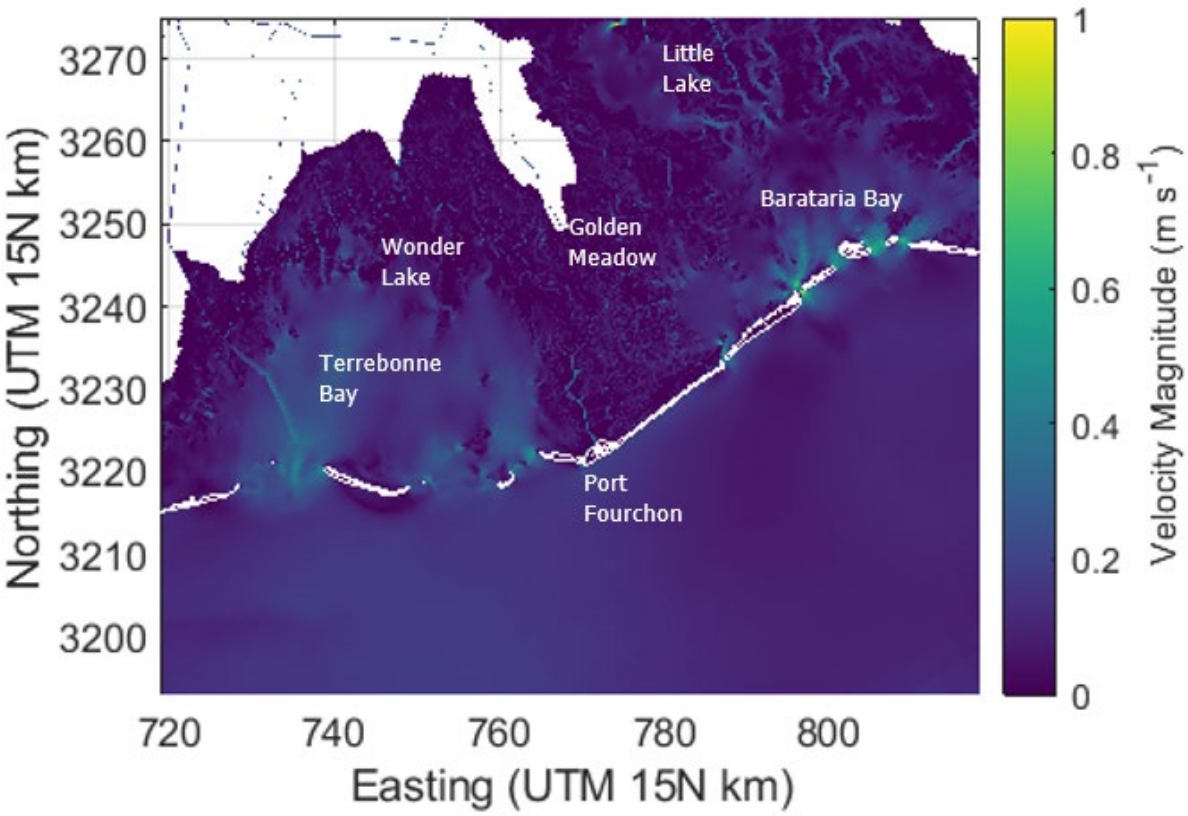

Figure B-33. Modeled flow velocities during a spring flood tide at 12:00 AM on January 5th, 2015

Waves

The wave model calibration assessed model skill in predicted wave heights during quiescent periods, cold fronts, and tropical cyclones Katrina and Rita. Wave and water level instrument deployments near Port Fourchon conducted to inform restoration project design provided data in the offshore and in Timbalier Bay (Coastal Engineering Consultants Inc., 2016). Additional data collected in the bay behind West Belle Headland (NAS-2C) for an unpublished study by the Institute was also used. Locations for wave and water level instrument deployments are shown in Figure B-34. Sample data is displayed in Figure B-35 and Figure B-36.

Figure B-34. Location of wave deployments from 2015 and 2019 that were used during calibration of the wave model. The interior bay site is from an unpublished study performed by the Institute in 2019. The offshore site is from a coastal restoration project design study in 2015.

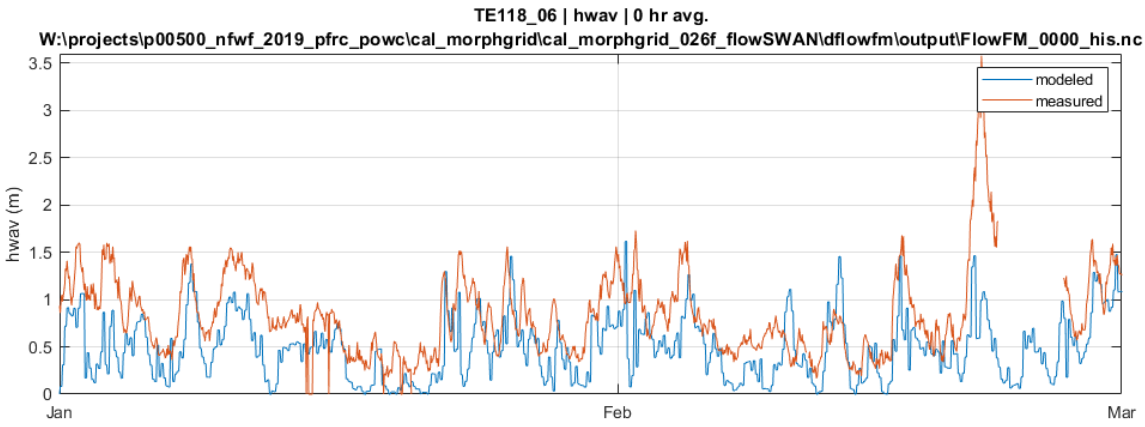

Figure B-35. Significant wave height at deployment site TE118_06 during January and February 2015

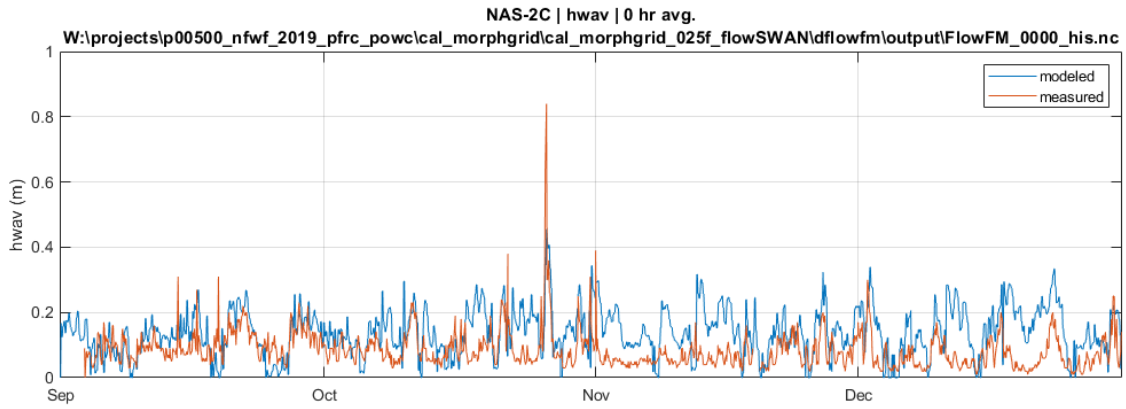

Figure B-36. Significant wave height at deployment site NAS-2C during fall and winter 2019

SALINITY

Calibration of salinity was performed after completing calibration of the hydrodynamics through adding sources of freshwater in the model and by adjusting the horizontal eddy diffusivity coefficient.

Freshwater Inflows

The main freshwater inflows that affect the model domain are indicated in Figure B-37. This section describes the calibration efforts separately for the Terrebonne Basin, Barataria Basin, and Mississippi River.

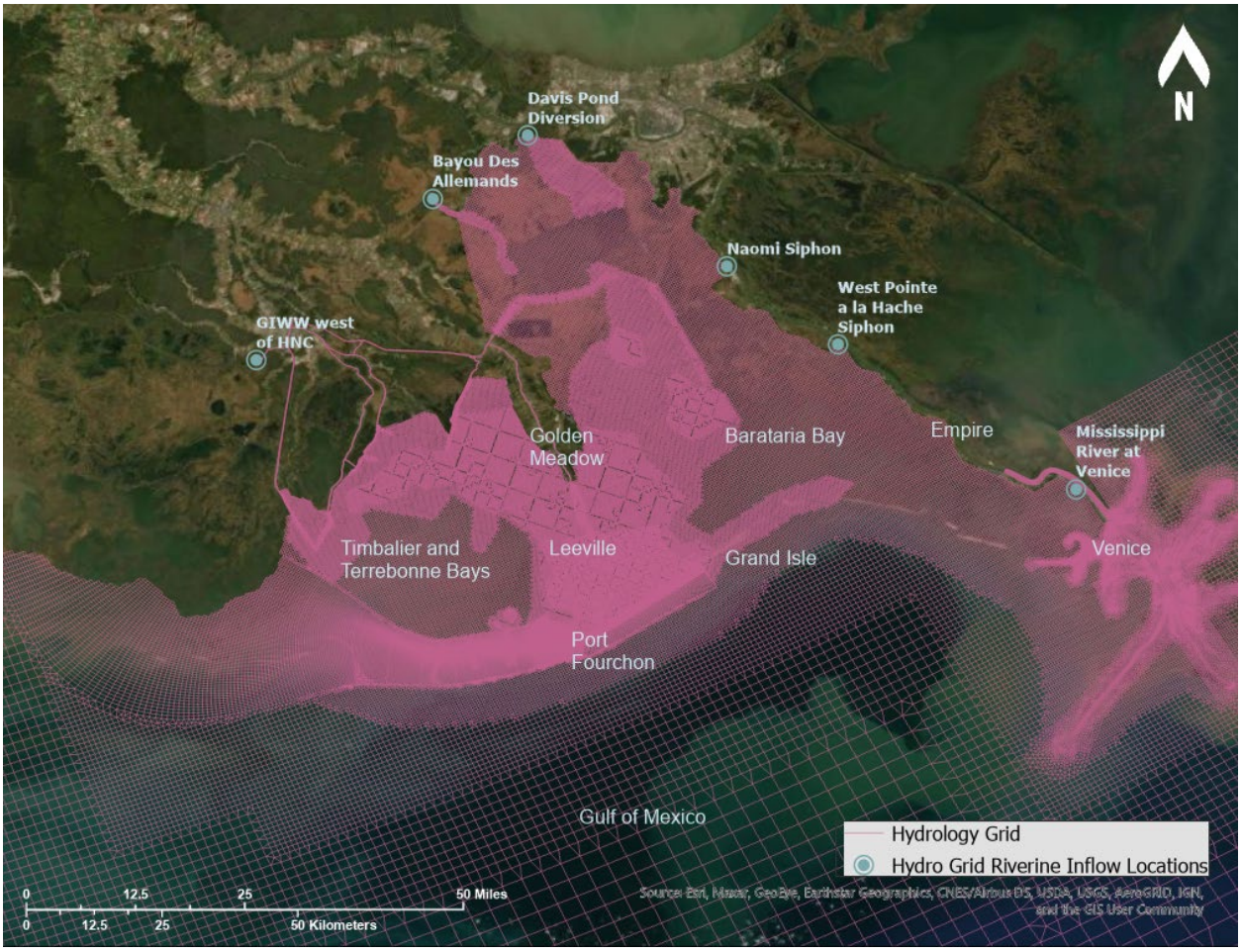

Figure B-37: Locations of freshwater inflows in the Hydrodynamics Model. Note that for clarity that labels are omitted for additional connections between the Gulf Intracoastal Waterway (GIWW) and the Terrebonne and Barataria basins. From west to east, these are the Houma Navigation Canal, Bayou Petit Caillou, Bayou Terrebonne, Grand Bayou Canal, and Bayou Lafourche.

Terrebonne Basin

The primary source of fresh water in the Terrebonne Basin is the Gulf Intracoastal Waterway (GIWW) which distributes freshwater from the Atchafalaya River. The relationship between stages in the Lower

Atchafalaya River (LAR) at Morgan City and discharge into the GIWW is described in the work of Swarenzski & Perrien (2015). Figure B-38 shows the correlation between the discharge in GIWW west of Houma Navigation Canal (HNC) and the stage of the Lower Atchafalaya River at Morgan City. A linear trendline was fitted in Figure B-38 to obtain a discharge timeseries for the GIWW west of HNC (Figure B-37) based on the 2015 and 2016 hydrographs of the LAR at Morgan City.

The Terrebonne Basin did not include additional discharges. Swarenzski & Perrien (2015) mention the importance of local rainfall runoff from the upper Terrebonne Basins. However, these inputs typically contribute much lower freshwater input than the discharge in the GIWW, except for periods with high local rainfall rates accompanied by low stages in the LAR. Therefore, quantifying freshwater releases for local rainfall would require a more focused analysis that is beyond the scope of this work.

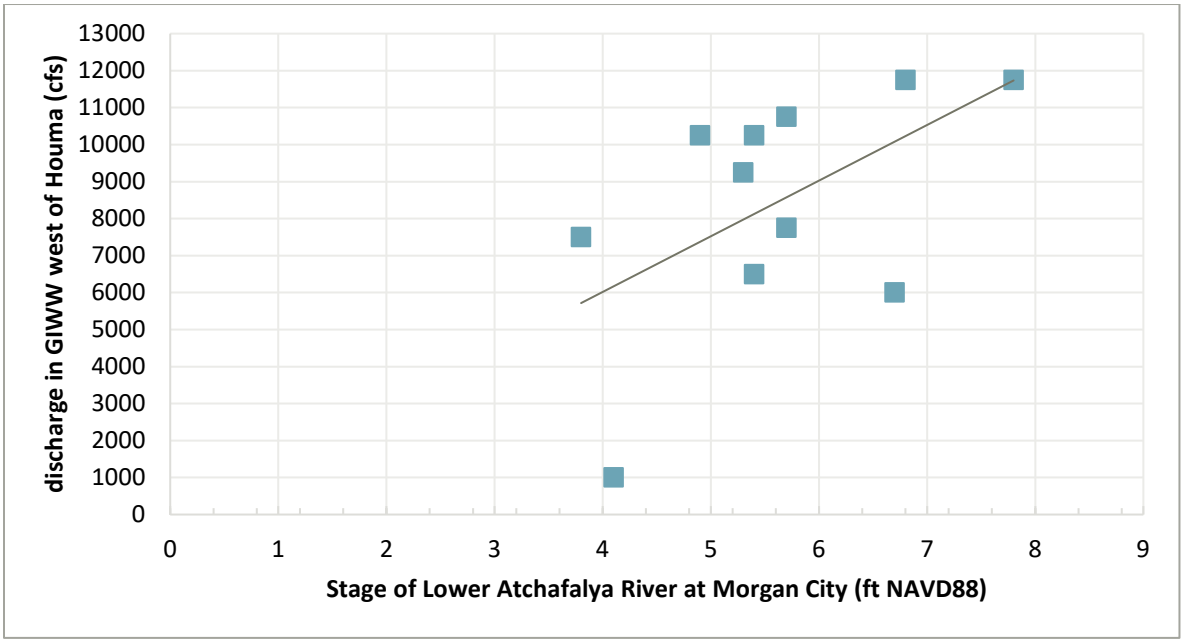

Figure B-38. Comparison of measured instantaneous discharge in the GIWW west of Houma in relation to measured stages of the Atchafalaya River at Morgan City. Data obtained from Swarenzski & Perrien (2015). Measurements were performed in 1997 and 1998, and 2007 and 2008.

The model grid resolves the distributary network connecting the GIWW to the Terrebonne Basin, as shown in Figure B-39. From west to east, these are the HNC, Bayou Petit Caillou, Bayou Terrebonne, Grand Bayou Canal, Bayou Lafourche, ending with the connection of the GIWW with the Barataria Basin east of Larose.

Calibration was done by adjusting the roughness in several channels to approximately match discharges along GIWW as presented by Swarenzski & Perrien (2015). To obtain realistic local salinity values at CRMS stations in the Terrebonne Basin close to channels that are part of the distributary network stemming from the GIWW. The resulting instantaneous and cumulative discharges are shown in Figure B-40 and Figure B-41, respectively.

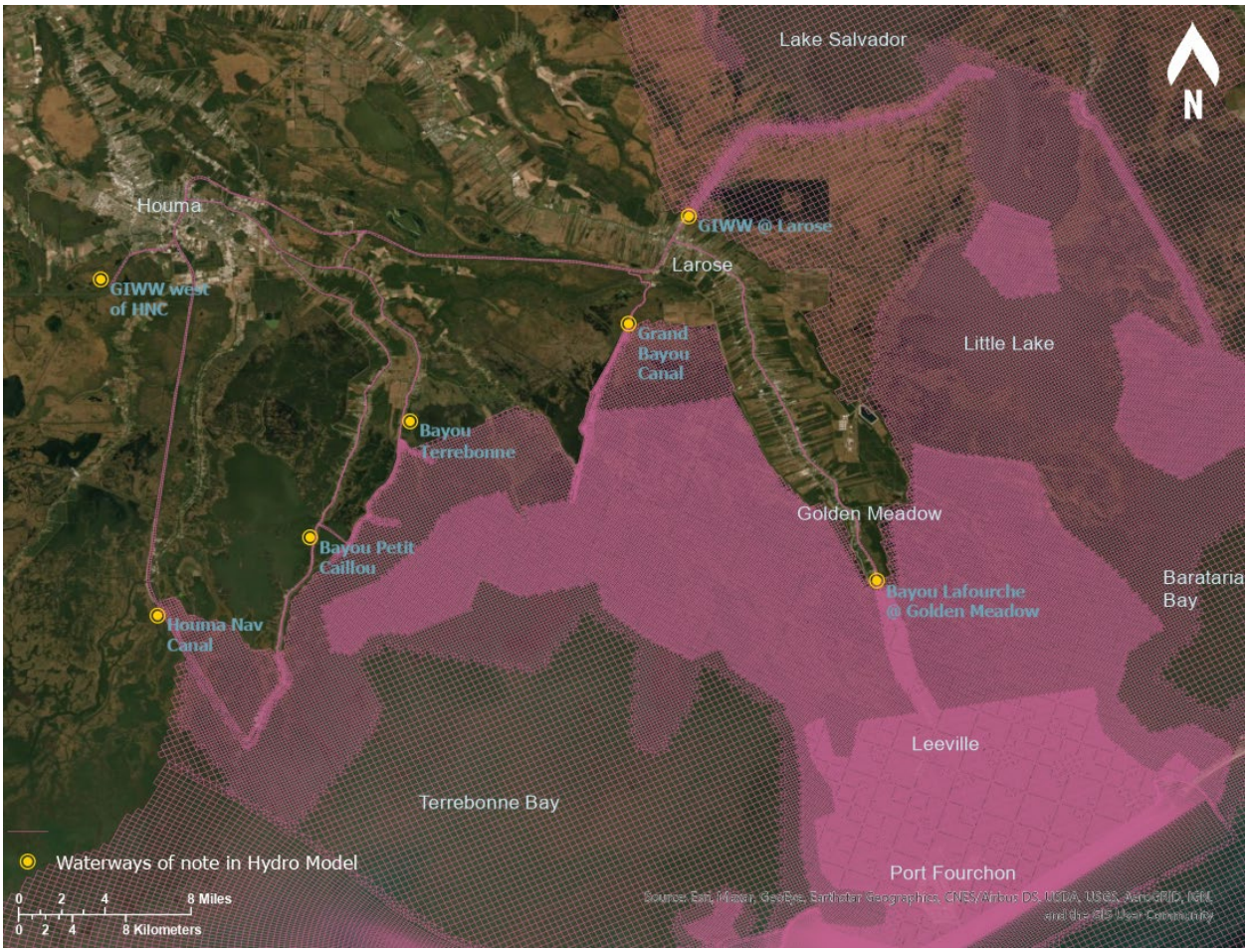

Figure B-39. Model grid showing the distributary network of channels connecting GIWW with the Barataria-Terrebonne Basin

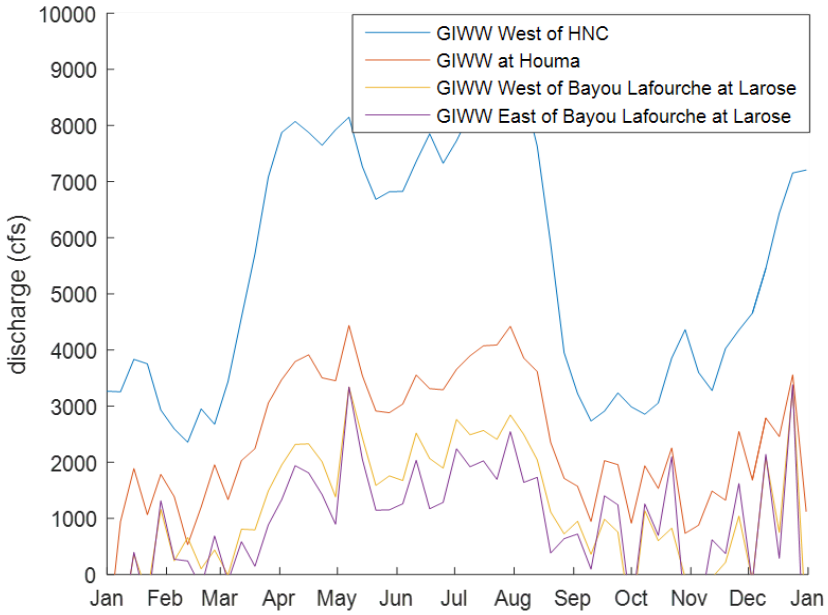

Figure B-40. Weekly average instantaneous discharges (cfs) for 2015 along the GIWW, ranging from the west (i.e. upstream) of HNC to where GIWW enters the Barataria Basin east of Bayou Lafourche at Larose

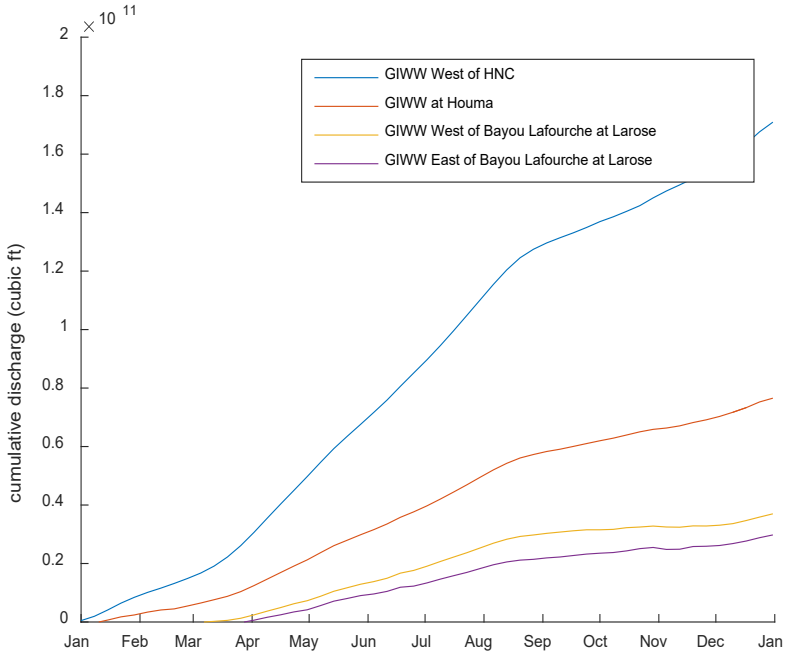

Figure B-41. Cumulative discharges (cubic feet) for 2015 along the GIWW, ranging from the west (i.e. upstream) of HNC to where GIWW enters the Barataria Basin east of Bayou Lafourche at Larose. Most of the discharge, i.e., about 55%, is drained through the HNC which is located between GIWW west of HNC and GIWW at Houma. About 25% is drained by Bayou Terrebonne, Bayou Petit Caillou, and Grand Canal, as can be seen from the difference between GIWW and Houma and GIWW West of Bayou Lafourche at Larose. The remaining 20% is mostly drained into the Barataria Basin, only a minor fraction of that drains through Bayou Lafourche.

Barataria Basin

The discharge of freshwater inflows in the Barataria Basin for 2015 are shown in Figure B-42. With the exception of the GIWW East of Bayou Lafourche at Larose discussed in the previous section, no adjustments were made to the freshwater inflow discharges obtained as described in the main report.

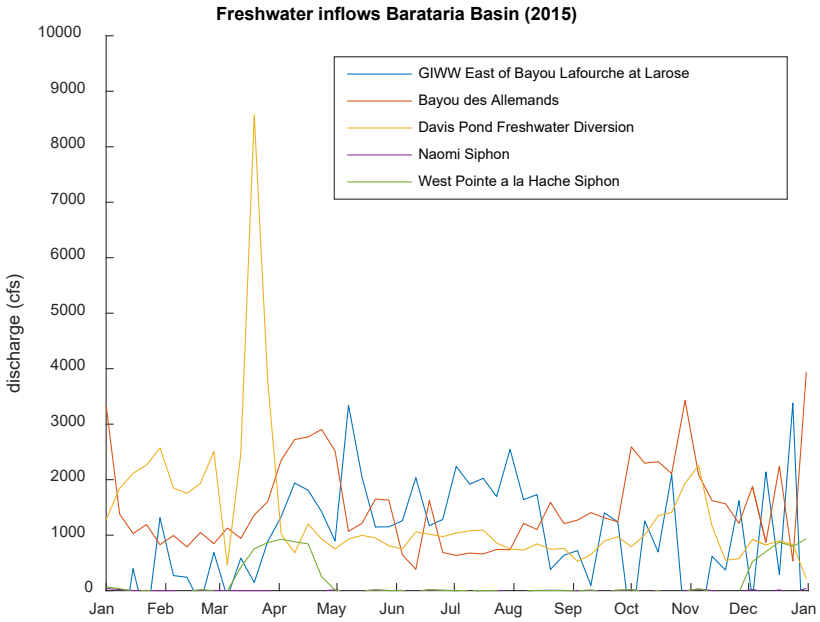

Figure B-42. Weekly average discharge of freshwater inflows into the Barataria Basin for 2015. The Naomi Siphon was not operated during this year

Mississippi River

Calibration of the Hydrodynamics Model with salinity was performed for years 2015 and 2016. The Mississippi River hydrographs are shown for both years in Figure B-43. Efforts to calibrate the model entailed adjustment of bathymetry and roughness in the distributary passes in the river's Modern Delta region (Figure B-44) to match distribution rates as documented in previous studies (McCorquodale et al., 2010). The outcomes are shown in

Table B-1.

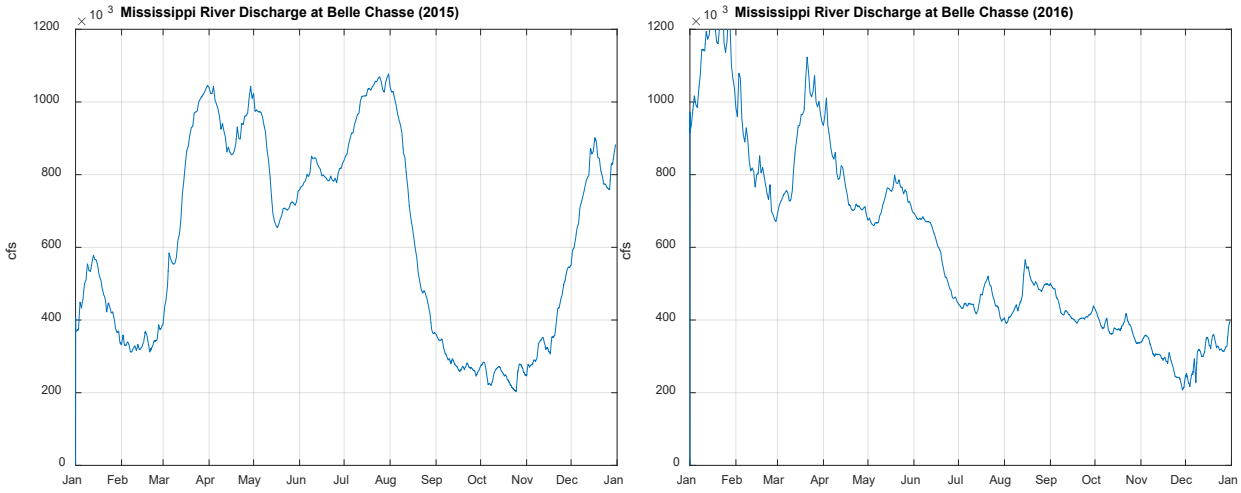

Figure B-43. Mississippi River hydrograph at Belle Chasse for years 2015 (left) and 2016 (right)

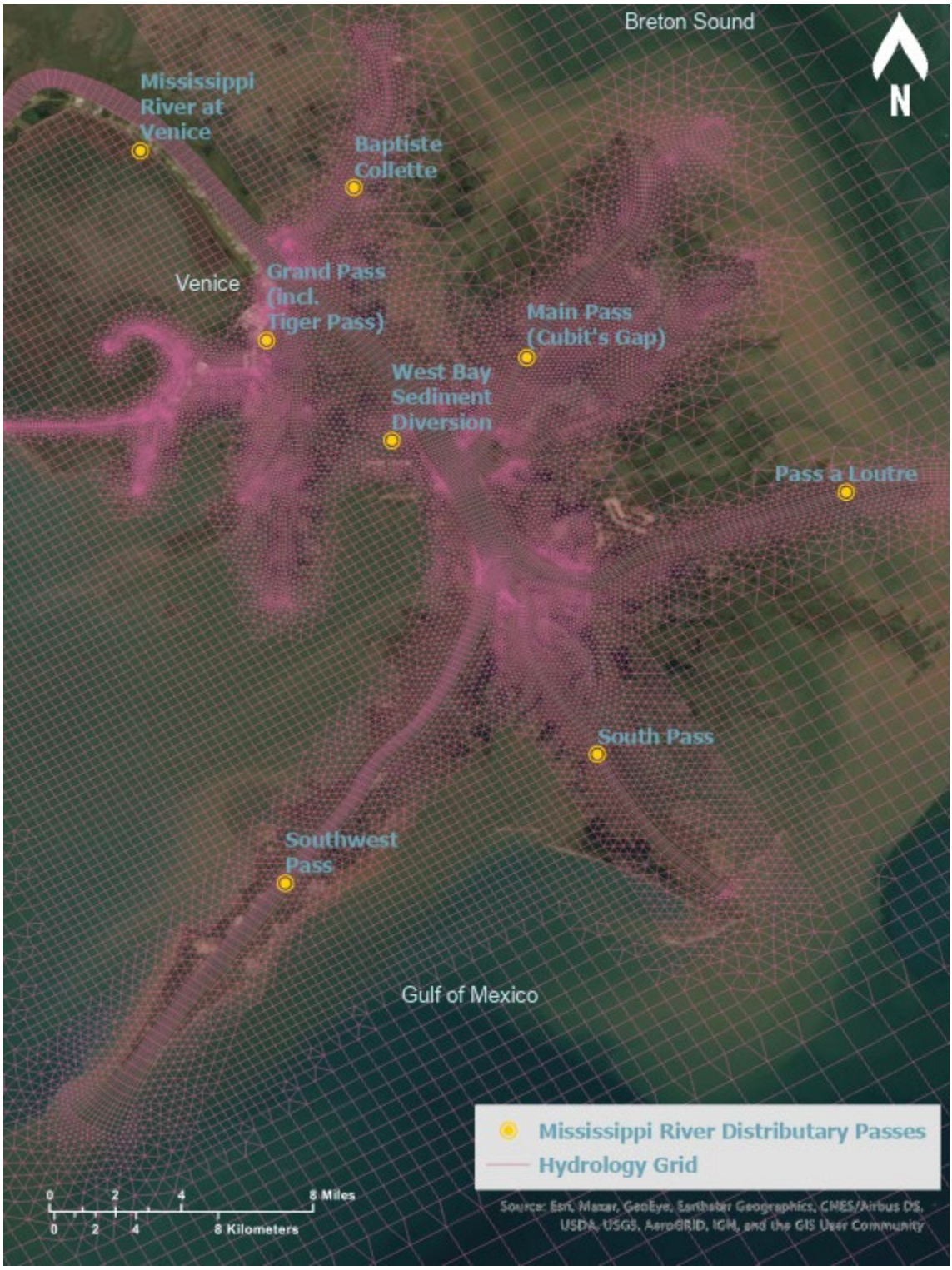

Figure B-44. Location of distributary passes in the Mississippi River's modern delta

Table B-1. Literature and modeled flow distribution rates through the Mississippi River's modern delta downstream of Venice. The rates from literature are based on McCorquodale (2010)

Distributary pass	Flow as percentage of total discharge at Venice	
	Literature	**Modeled**
Baptiste Collette	16%	14%
Grand Pass (including Tiger Pass)	11%	12%
Main Pass (Cubit's Gap)	11%	10%
Pass A Loutre	8%	10%
South Pass	15%	12%
Southwest Pass	35%	34%
West Bay Sediment Diversion	5%	6%

Salinity Timeseries

This section contains comparisons between modeled and measured salinity at open water gauges from USGS and CRMS wetland gauges located across the Barataria-Terrebonne Basin (Figure B-45). Results are shown for each area or region, i.e., the Port Fourchon Area, Lower Barataria, Mid-Barataria, Upper Barataria, Lower and Mid-Terrebonne, and Upper Terrebonne, for years 2015 and 2016.

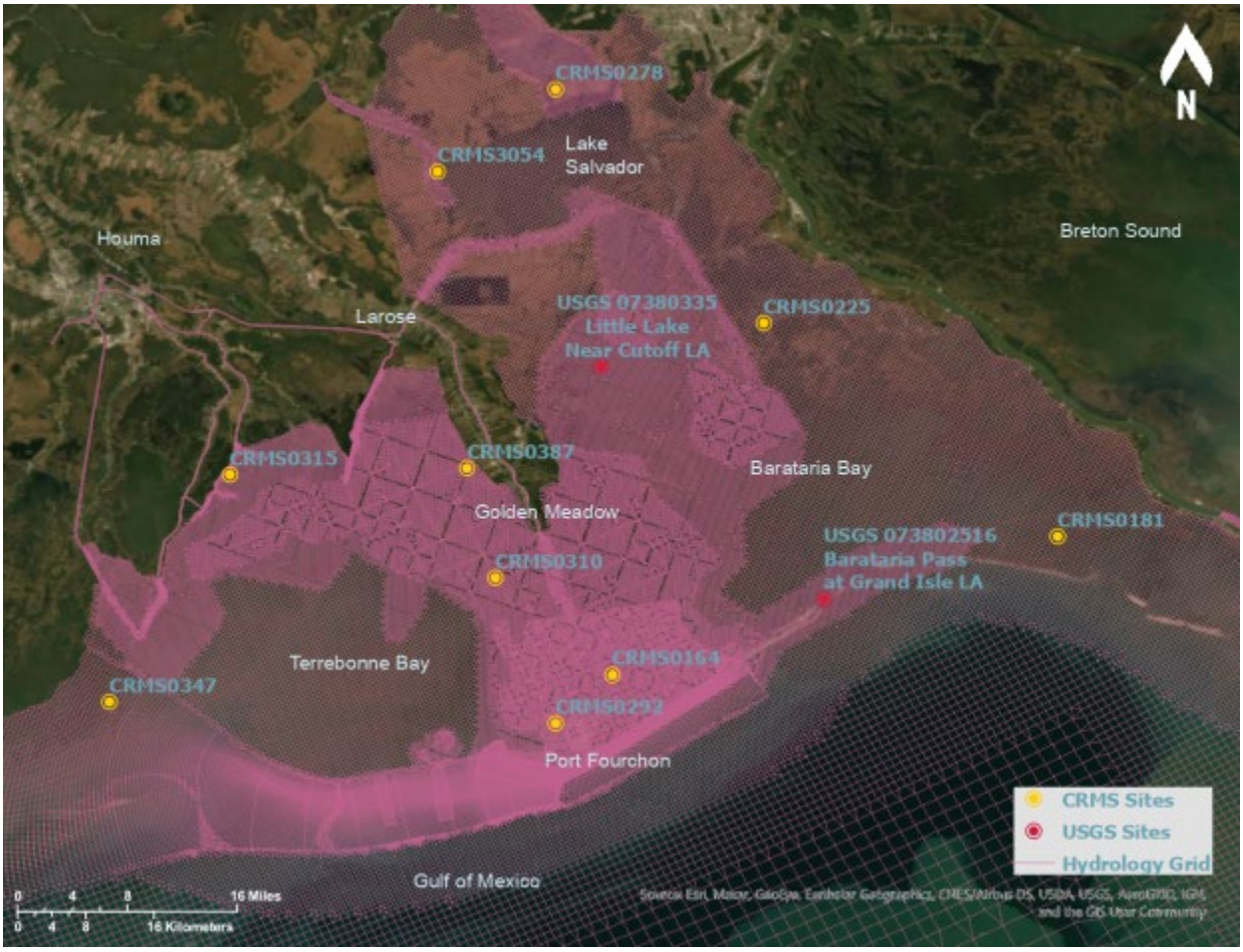

Figure B-45. Location of USGS and CRMS stations used in the model calibration of water level (Figure B-46 through Figure B-69).

Port Fourchon Area

2015

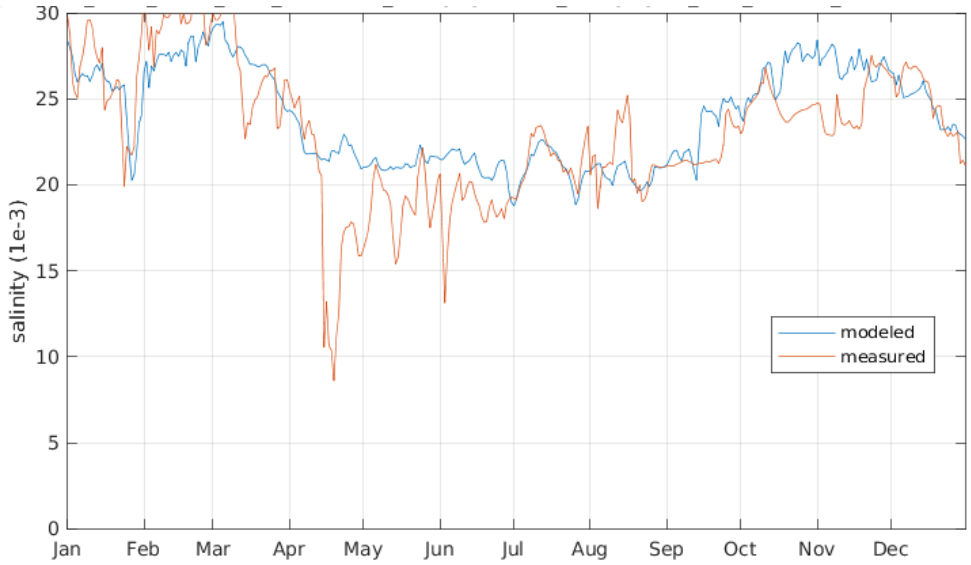

Figure B-46. Salinity timeseries comparison (ppt, daily averaged) for 2015 at CMRS0292

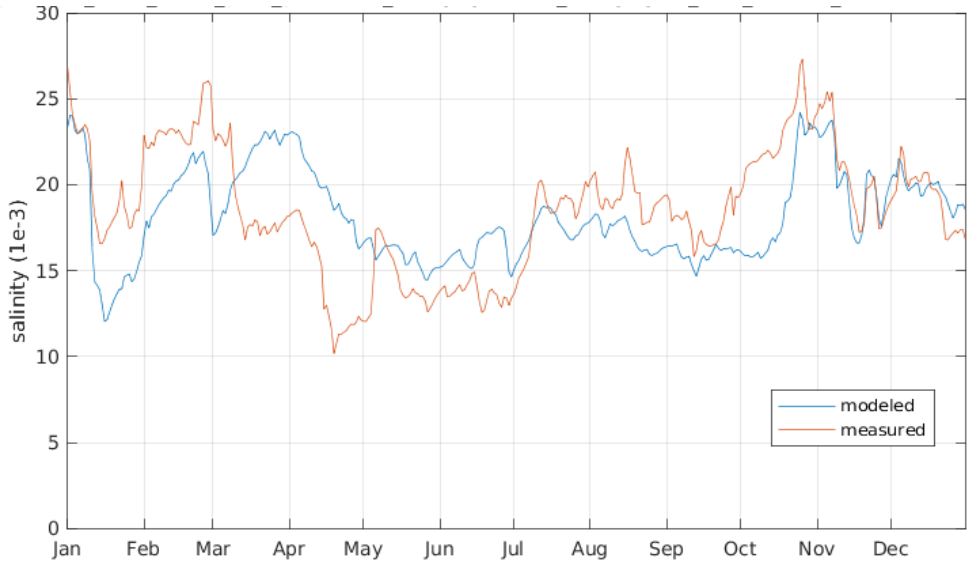

Figure B-47. Salinity timeseries comparison (ppt, daily averaged) for 2015 at CMRS0164

2016

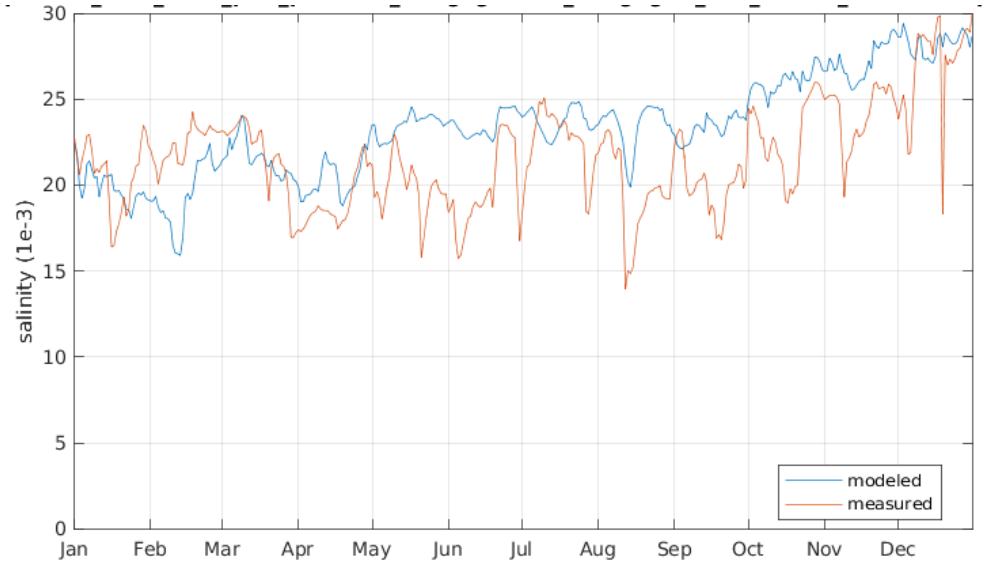

Figure B-48. Salinity timeseries comparison (ppt, daily averaged) for 2016 at CMRS0292

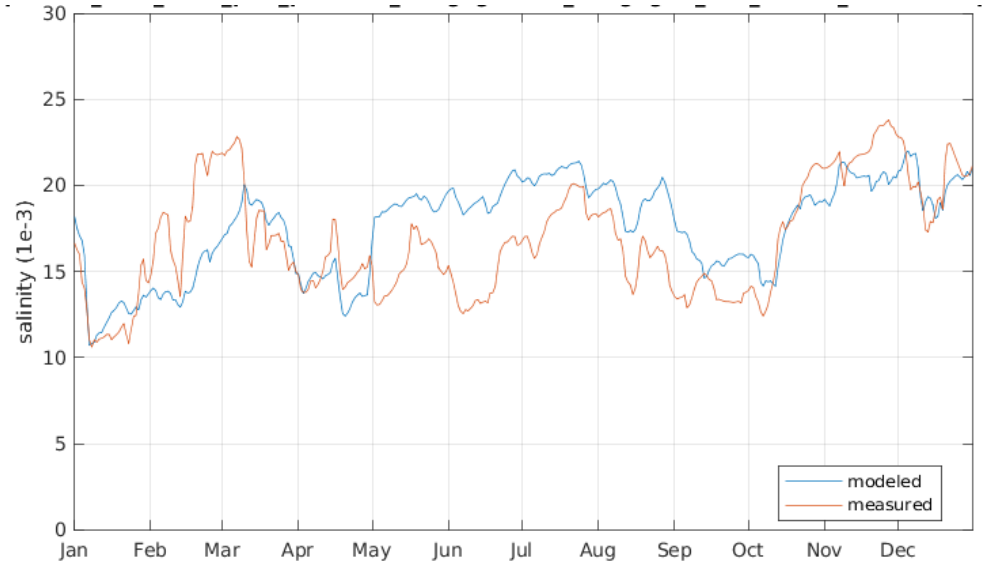

Figure B-49. Salinity timeseries comparison (ppt, daily averaged) for 2016 at CMRS0164

Lower Barataria

2015

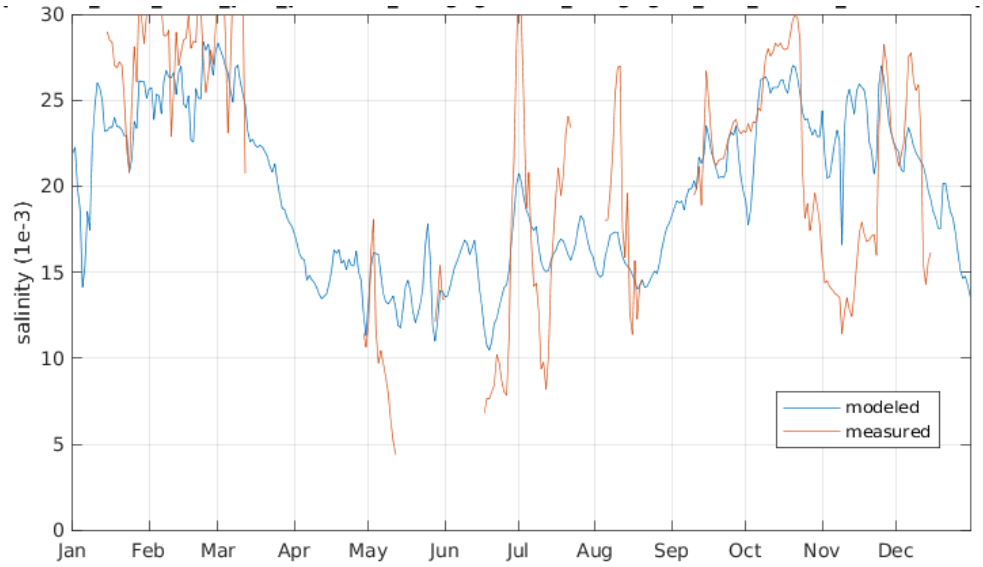

Figure B-50. Salinity timeseries comparison (ppt, daily averaged) for 2015 at USGS 073802516 Barataria Pass at Grand Isle

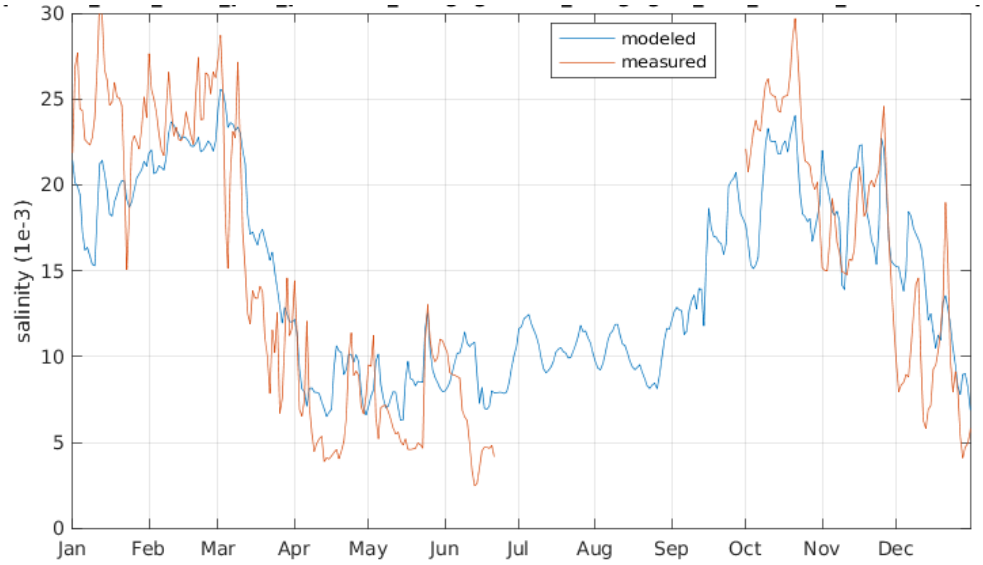

Figure B-51. Salinity timeseries comparison (ppt, daily averaged) for 2015 at CRMS0181

2016

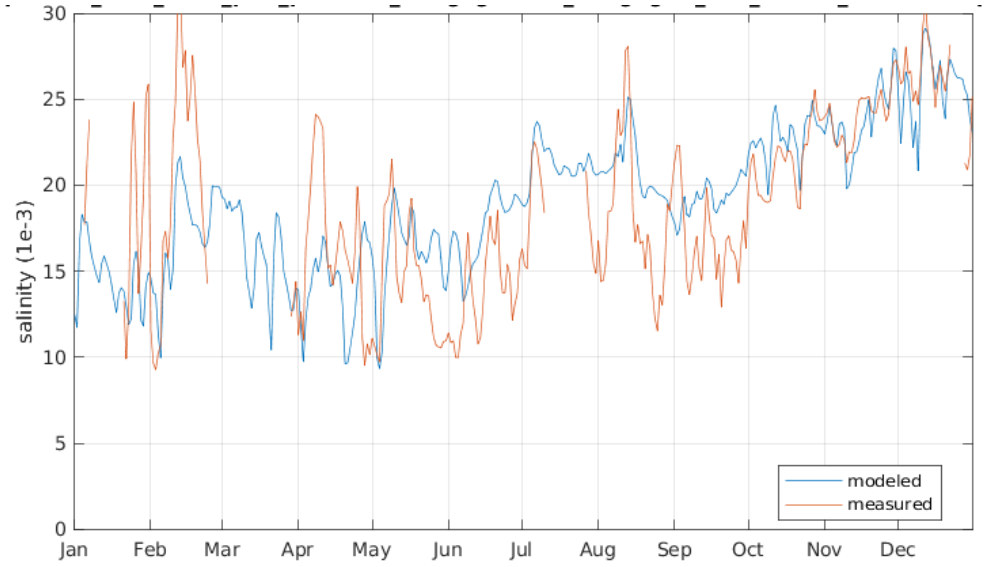

Figure B-52. Salinity timeseries comparison (ppt, daily averaged) for 2016 at USGS 073802516 Barataria Pass at Grand Isle

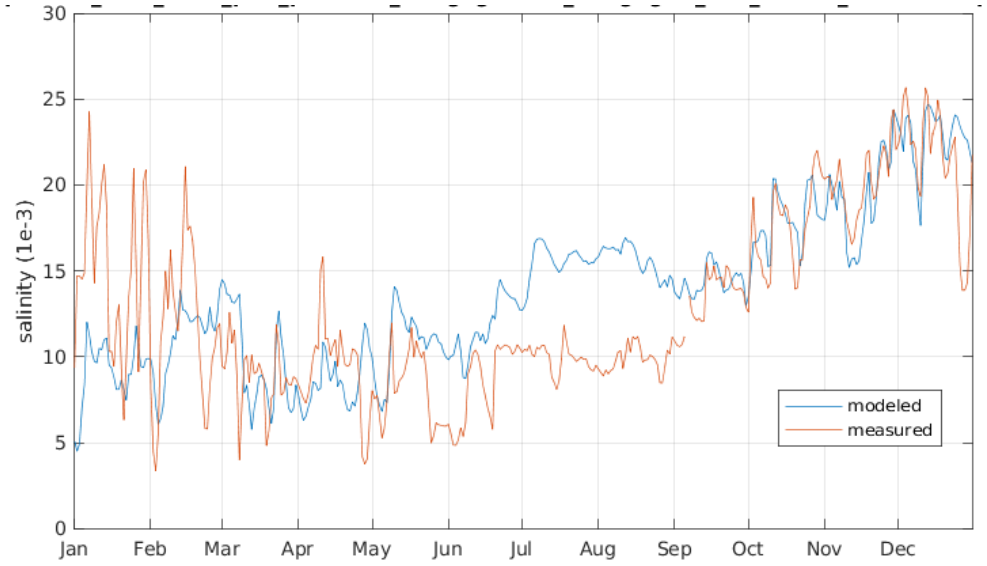

Figure B-53. Salinity timeseries comparison (ppt, daily averaged) for 2016 at CRMS0181

Mid-Barataria

2015

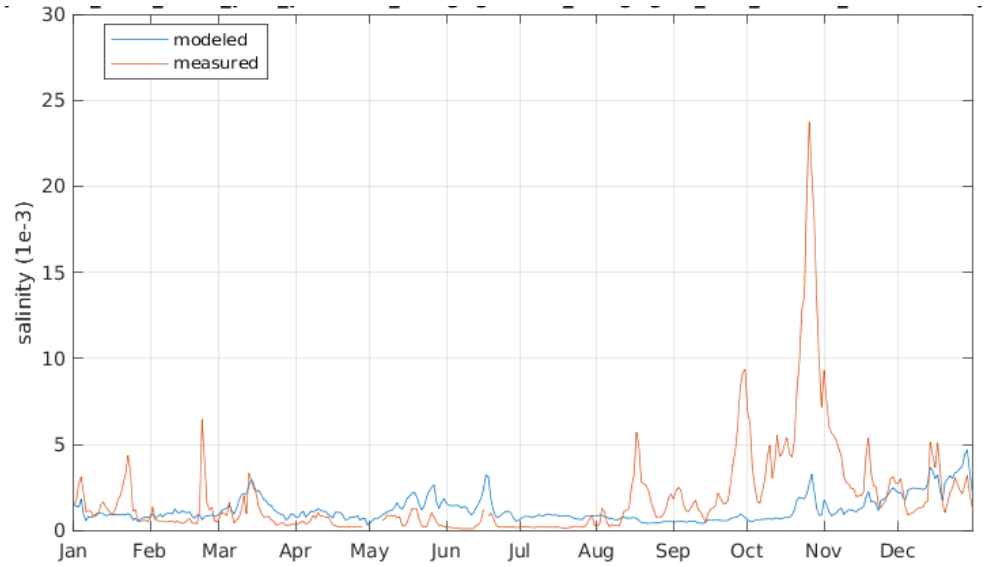

Figure B-54. Salinity timeseries comparison (ppt, daily averaged) for 2015 at USGS 07380335 Little Lake Near Cutoff

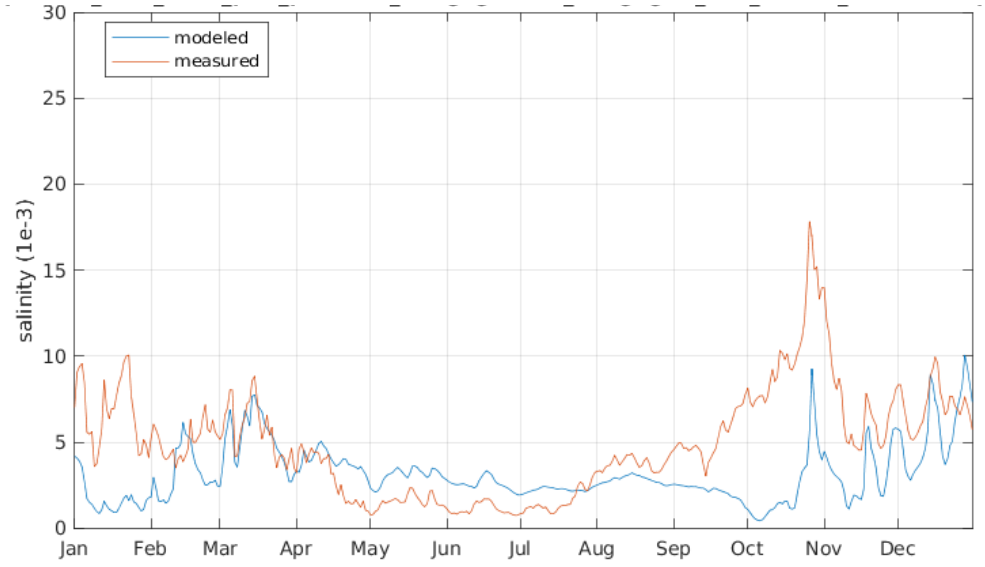

Figure B-55. Salinity timeseries comparison (ppt, daily averaged) for 2015 at CRMS0225

2016

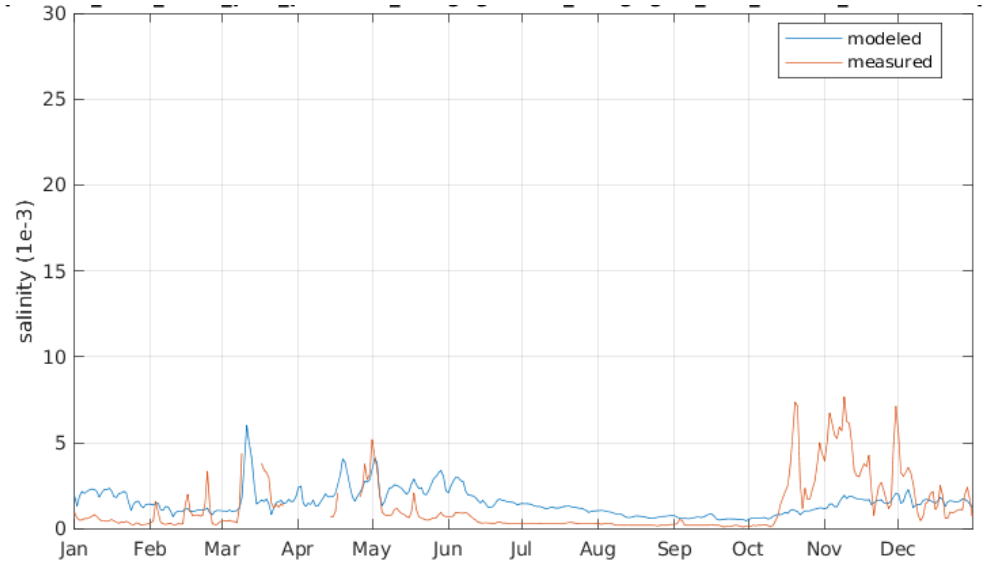

Figure B-56. Salinity timeseries comparison (ppt, daily averaged) for 2016 at USGS 07380335 Little Lake Near Cutoff

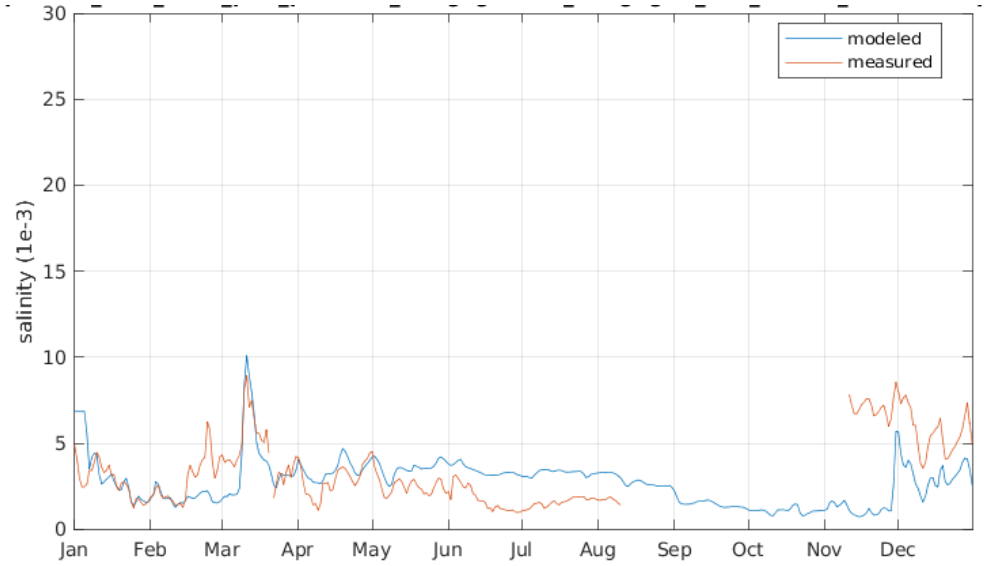

Figure B-57. Salinity timeseries comparison (ppt, daily averaged) for 2016 at CRMS0225

Upper Barataria

2015

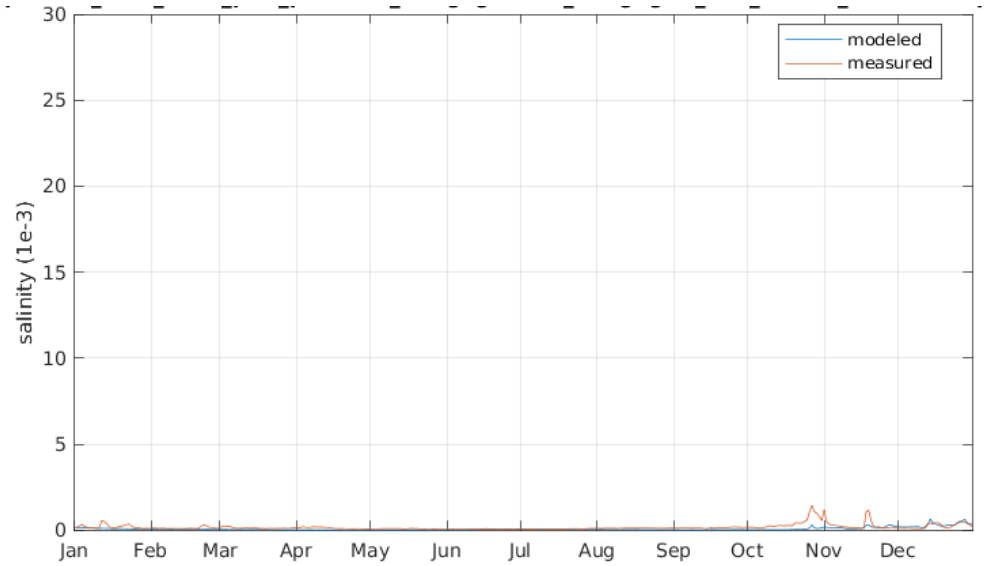

Figure B-58. Salinity timeseries comparison (ppt, daily averaged) for 2015 at CRMS3054

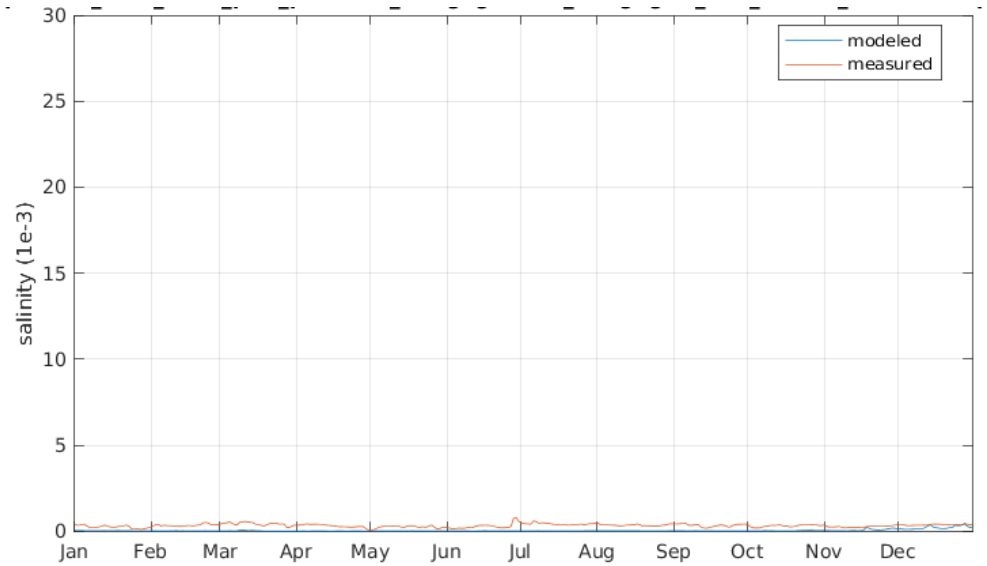

Figure B-59. Salinity timeseries comparison (ppt, daily averaged) for 2015 at CRMS0278

2016

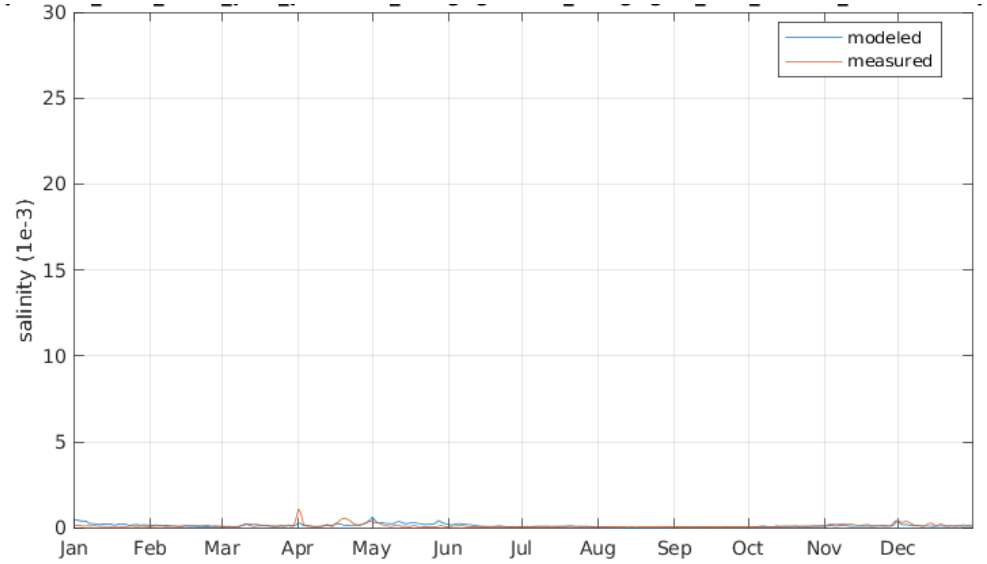

Figure B-60. Salinity timeseries comparison (ppt, daily averaged) for 2016 at CRMS3054

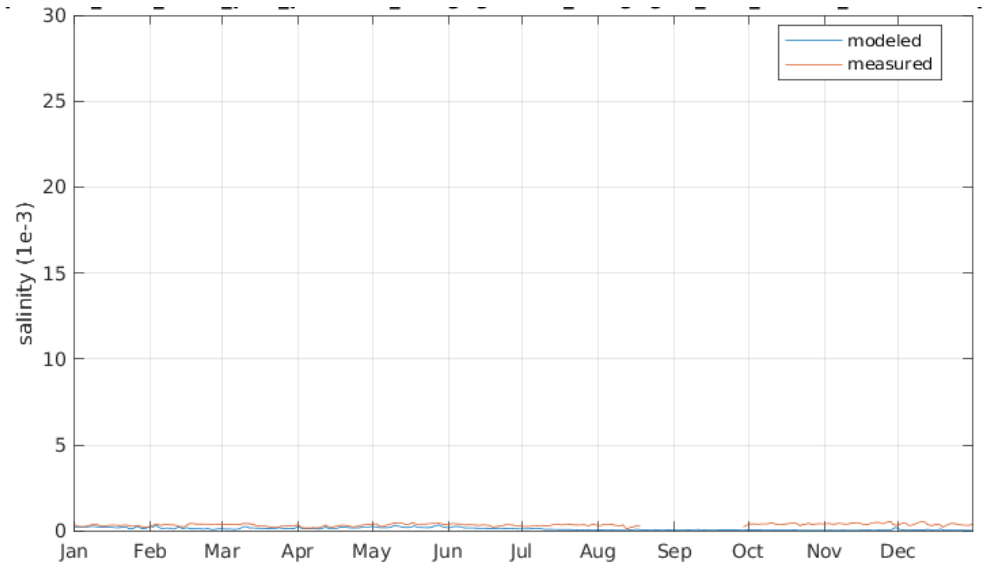

Figure B-61. Salinity timeseries comparison (ppt, daily averaged) for 2016 at CRMS0278

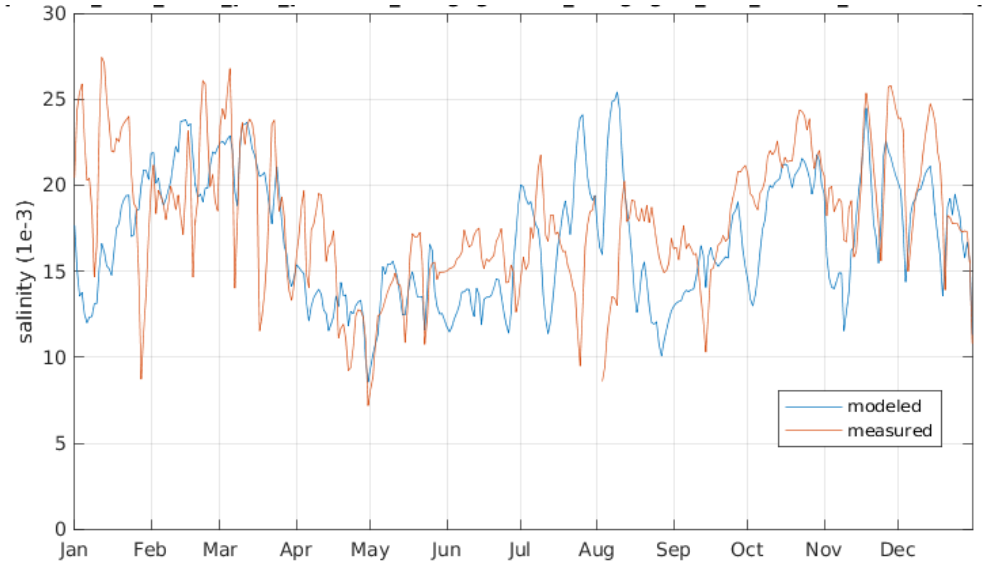

Figure B-62. Salinity timeseries comparison (ppt, daily averaged) for 2015 at CRMS0347

Figure B-63. Salinity timeseries comparison (ppt, daily averaged) for 2015 at CRMS0310

2016

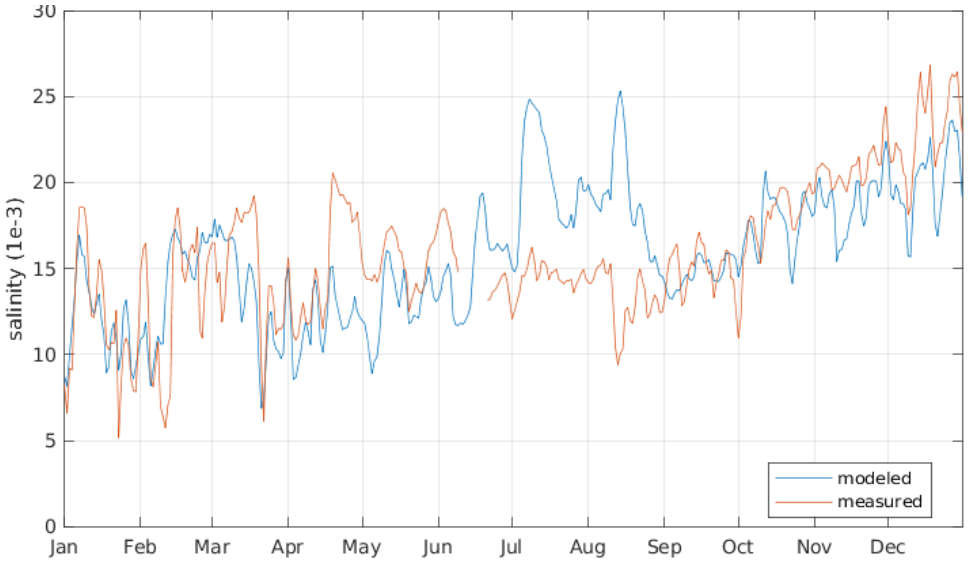

Figure B-64. Salinity timeseries comparison (ppt, daily averaged) for 2016 at CRMS0347

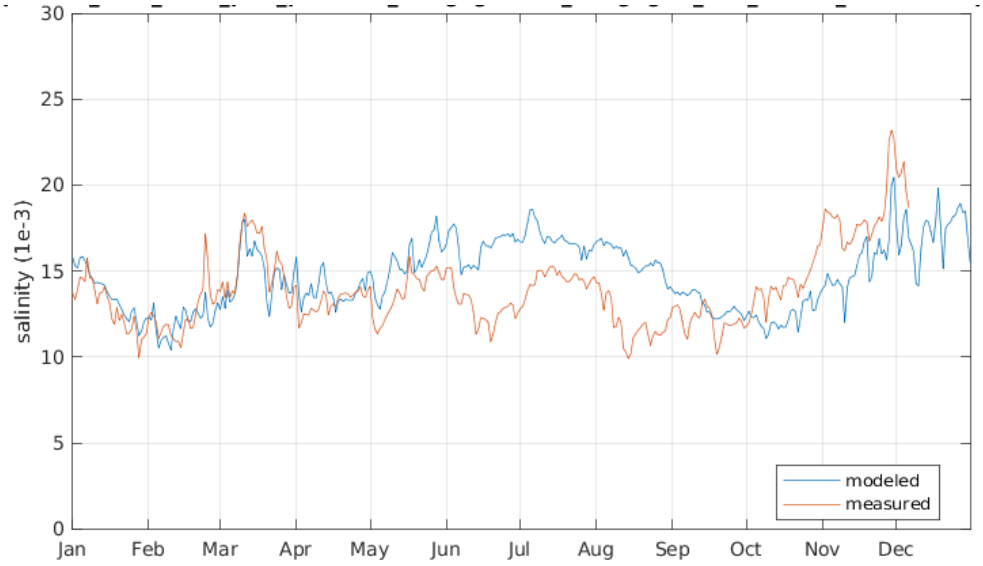

Figure B-65. Salinity timeseries comparison (ppt, daily averaged) for 2016 at CRMS0310

Upper Terrebonne

2015

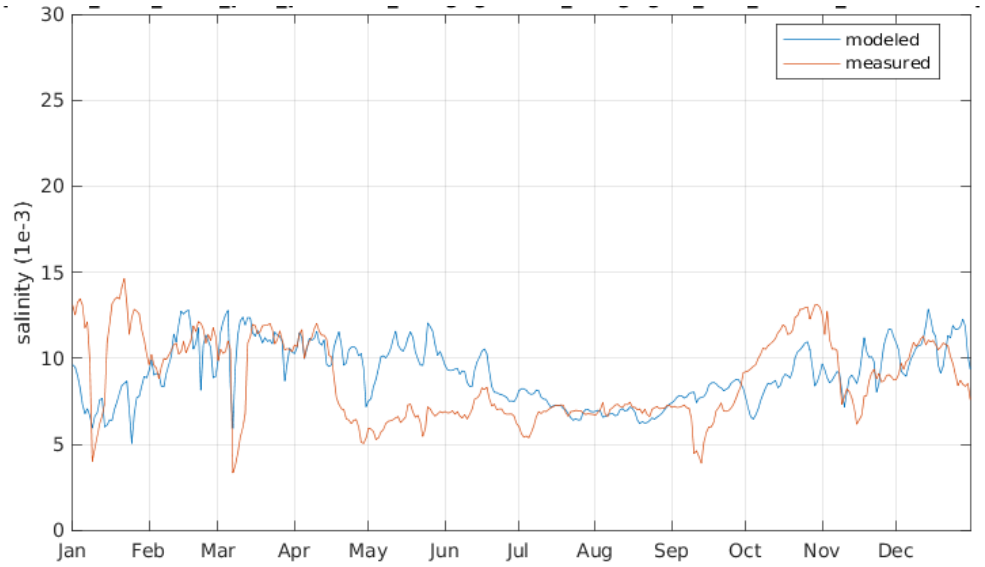

Figure B-66. Salinity timeseries comparison (ppt, daily averaged) for 2015 at CRMS0315

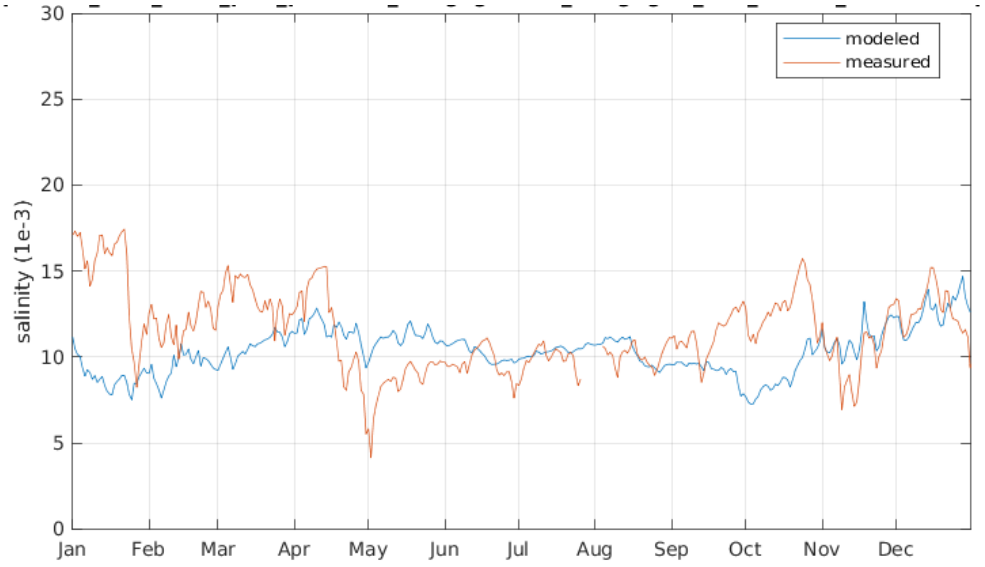

Figure B-67. Salinity timeseries comparison (ppt, daily averaged) for 2015 at CRMS0387

2016

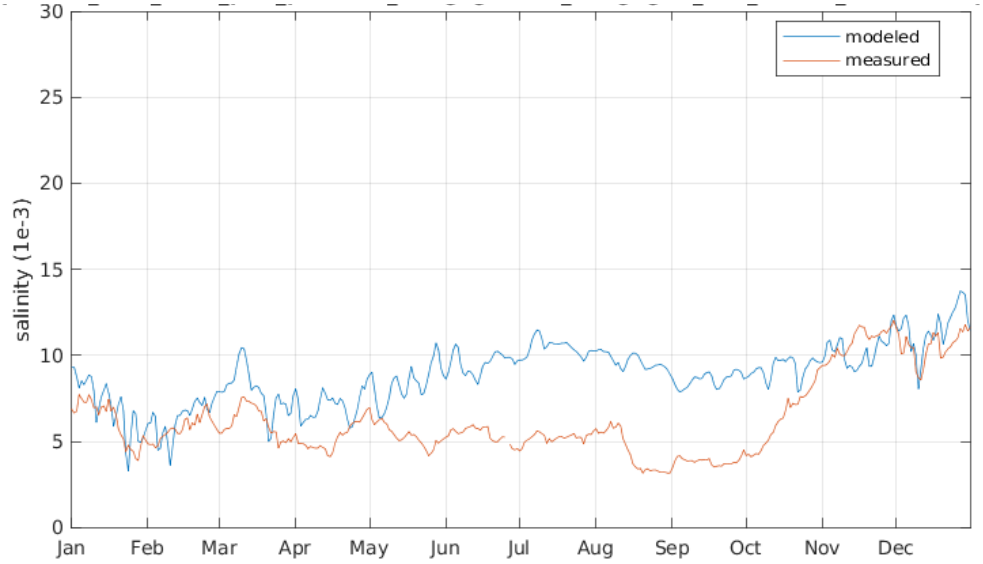

Figure B-68. Salinity timeseries comparison (ppt, daily averaged) for 2016 at CRMS0315

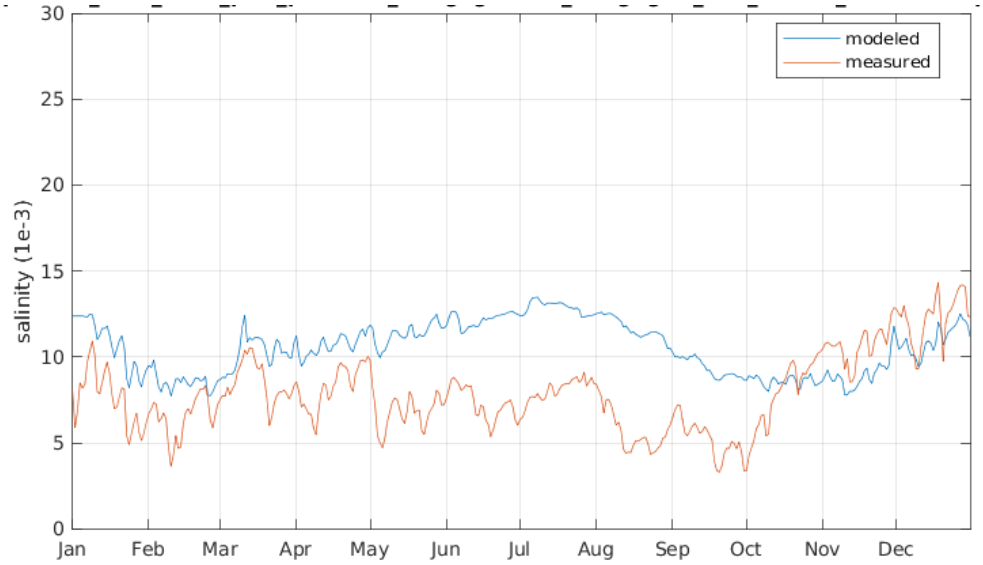

Figure B-69. Salinity timeseries comparison (ppt, daily averaged) for 2016 at CRMS0387

LITERATURE CITED

Coastal Engineering Consultants Inc. (2016). *TE-118 East Timbalier Island Restoration Project: Numerical modeling of restoration alternatives* (Draft No. CEC File No. 15.225) (p. 102). Baton Rouge, LA: Coastal Engineering Consultants Inc. Prepared for Coastal Protection and Restoration Authority.

Cobell, Z., & Roberts, H. (2021). *Storm surge and waves: model updates for the 2023 Coastal Master Plan* (No. Version 1) (p. 56). Coastal Protection and Restoration Authority.

Escoffier, F. (1940). The Stability of Tidal Inlets. *Shore and Beach*, *8*(4).

Huang, W., & Li, C. (2020). Contrasting Hydrodynamic Responses to Atmospheric Systems with Different Scales: Impact of Cold Fronts vs. That of a Hurricane. *Journal of Marine Science and Engineering*.

McCorquodale, A., Georgiou, I., Davis, M. D., & Pereira, J. (2010). *Hydrology and Hydrodynamic Modeling of the Mississippi River in Southeast Louisiana*. New Orleans, LA: Pontchartrain Institute for Environmental Studies, University of New Orleans.

NOAA. (n.d.). Sea Level Trends - NOAA Tides & Currents.

Pawlowicz, R., Beardsley, B., & Lentz, S. (2002). Classical tidal harmonic analysis including error estimates in MATLAB using T_TIDE. *Computers and Geosciences*, *28*.

Swarenzski, C. M., & Perrien, S. M. (2015). *Discharge, Suspended Sediment, and Salinity in the Gulf Intracoastal Waterway and Adjacent Surface Waters in South-Central Louisiana, 1997–2008* (Scientific Investigations Report No. 2015–5132) (p. 30). Reston, Virginia: U.S. Geological Survey.